

# SANDIA REPORT

SAND2010-6918

Unlimited Release

Printed October 2010

## Discontinuous Galerkin Finite Element Methods for Gradient Plasticity

Jakob Ostien, Krishna Garikipati

Prepared by

Sandia National Laboratories

Albuquerque, New Mexico 87185 and Livermore, California 94550

Sandia National Laboratories is a multi-program laboratory managed and operated by Sandia Corporation, a wholly owned subsidiary of Lockheed Martin Corporation, for the U.S. Department of Energy's National Nuclear Security Administration under contract DE-AC04-94AL85000.

Approved for public release; further dissemination unlimited.



**Sandia National Laboratories**

Issued by Sandia National Laboratories, operated for the United States Department of Energy by Sandia Corporation.

**NOTICE:** This report was prepared as an account of work sponsored by an agency of the United States Government. Neither the United States Government, nor any agency thereof, nor any of their employees, nor any of their contractors, subcontractors, or their employees, make any warranty, express or implied, or assume any legal liability or responsibility for the accuracy, completeness, or usefulness of any information, apparatus, product, or process disclosed, or represent that its use would not infringe privately owned rights. Reference herein to any specific commercial product, process, or service by trade name, trademark, manufacturer, or otherwise, does not necessarily constitute or imply its endorsement, recommendation, or favoring by the United States Government, any agency thereof, or any of their contractors or subcontractors. The views and opinions expressed herein do not necessarily state or reflect those of the United States Government, any agency thereof, or any of their contractors.

Printed in the United States of America. This report has been reproduced directly from the best available copy.

Available to DOE and DOE contractors from  
U.S. Department of Energy  
Office of Scientific and Technical Information  
P.O. Box 62  
Oak Ridge, TN 37831

Telephone: (865) 576-8401  
Facsimile: (865) 576-5728  
E-Mail: [reports@adonis.osti.gov](mailto:reports@adonis.osti.gov)  
Online ordering: <http://www.osti.gov/bridge>

Available to the public from  
U.S. Department of Commerce  
National Technical Information Service  
5285 Port Royal Rd  
Springfield, VA 22161

Telephone: (800) 553-6847  
Facsimile: (703) 605-6900  
E-Mail: [orders@ntis.fedworld.gov](mailto:orders@ntis.fedworld.gov)  
Online ordering: <http://www.ntis.gov/help/ordermethods.asp?loc=7-4-0#online>



# Discontinuous Galerkin Finite Element Methods for Gradient Plasticity

Jakob Ostien  
Mechanics of Materials  
Sandia National Laboratories  
P.O. Box 969  
Livermore, CA 94551  
jtostie@sandia.gov

Krishna Garikipati  
Department of Mechanical Engineering  
University of Michigan  
2350 Hayward Street  
Ann Arbor, MI 48109  
krishna@umich.edu

## Abstract

In this report we apply discontinuous Galerkin finite element methods to the equations of an incompatibility based formulation of gradient plasticity. The presentation is motivated with a brief overview of the description of dislocations within a crystal lattice. A tensor representing a measure of the incompatibility with the lattice is used in the formulation of a gradient plasticity model. This model is cast in a variational formulation, and discontinuous Galerkin machinery is employed to implement the formulation into a finite element code. Finally numerical examples of the model are shown.



# Contents

<b>1</b>	<b>Introduction</b>	<b>9</b>
1.1	Background .....	9
1.2	An Overview .....	13
<b>2</b>	<b>Dislocation Based Plasticity</b>	<b>15</b>
2.1	Plasticity in Crystals .....	15
2.2	Extending Burger's Vector to the Continuum .....	22
<b>3</b>	<b>Gradient Plasticity Model</b>	<b>25</b>
<b>4</b>	<b>Variational Formulation</b>	<b>29</b>
<b>5</b>	<b>Implementation</b>	<b>33</b>
5.1	Mixed Plasticity .....	33
5.2	Constant Basis for $\mathbf{H}^p$ .....	38
5.3	Linear Basis for $\mathbf{H}^p$ .....	40
<b>6</b>	<b>Results</b>	<b>43</b>
6.1	Mixed Plasticity .....	43
6.2	Constant Basis for $\mathbf{H}^p$ .....	49
6.3	Linear Basis for $\mathbf{H}^p$ .....	54
<b>7</b>	<b>Conclusions</b>	<b>57</b>
	<b>References</b>	<b>59</b>

# List of Figures

2.1	Common metal crystals: a) FCC, b) BCC, c) HCP . . . . .	16
2.2	Slip plane in a body under uniaxial tension . . . . .	17
2.3	Relative displacement of a whole plane of atoms . . . . .	17
2.4	An edge dislocation with Burger's vector, $\mathbf{b}$ . . . . .	18
2.5	A screw dislocation . . . . .	19
2.6	Edge dislocation moving through a lattice . . . . .	19
2.7	A Frank-Read source for dislocation generation . . . . .	21
6.1	Schematic of the torsion BVP . . . . .	44
6.2	Perfect plasticity for the torsion BVP . . . . .	45
6.3	Isotropic hardening for the torsion BVP . . . . .	46
6.4	Schematic of the plane strain compression BVP . . . . .	47
6.5	Softening in the plane strain compression BVP . . . . .	47
6.6	Equivalent plastic strain for each mesh . . . . .	48
6.7	Picture of Mesh 3 for the DG torsion problem . . . . .	50
6.8	Hardening curve for various mesh densities . . . . .	50
6.9	Influence of hardening modulus on torque versus twist . . . . .	51
6.10	No hardening for model in tension . . . . .	52
6.11	Size effect of varying the cylinder radius . . . . .	53
6.12	Mesh dependent softening . . . . .	53
6.13	Mesh independent softening via the gradient model . . . . .	54
6.14	Pressure field in plane strain . . . . .	55
6.15	Equivalent plastic strain field in plane strain . . . . .	56

# List of Tables

2.1	Examples of FCC, BCC, and HCP metals . . . . .	16
6.1	Parameters used in the simulation of the torsion BVP . . . . .	44
6.2	Number of elements per mesh for the torsion BVP . . . . .	45
6.3	Number of elements per mesh for the plane strain compression BVP . . . . .	48
6.4	Number of elements per mesh for the DG torsion problem . . . . .	49



# Chapter 1

## Introduction

The purpose of this work is to present a numerical method for solving the partial differential equations that arise from a variationally-derived model of gradient plasticity. The main focus is the employment of discontinuous Galerkin finite element principles to alleviate the strict continuity requirements that arise from the classical statement of the gradient plasticity problem in weak form. The model of gradient plasticity chosen for this work is physically motivated by considering the incompatibilities brought about by plastic deformation at the microscopic scale, and manipulated via Stokes' Theorem to obtain a continuum, tensorial treatment. Integration algorithms resembling those from the nonlinear classical theory of plasticity are used to solve a pair of partial differential equations that amount to the macroscopic and microscopic equations of equilibrium. Some numerical examples are used to demonstrate properties of the model and the method. Algorithms for approximating the back-stress term in the yield condition are investigated, as well as integration algorithms for the mixed method.

### 1.1 Background

The theory of *plasticity* covers the response of materials that have experienced loads exceeding their elastic limit, or outside of the realm in which the material can be expected to fully recover to its original configuration. The material retains a permanent distortion by some measure, and this distortion is governed by an irreversible, or dissipative, process. The physics underlying plastic deformation on a microscopic scale dictates the mechanical behavior of a material at the macroscopic scale, but is generally too complex to be modeled directly, and therefore phenomenological models are usually employed.

The history of the theory of plasticity began with attempts to describe the permanent deformation observed in metals that had experienced loads exceeding their elastic limit. Metals are generally polycrystalline materials, and at a microscopic scale plastic deformation results in changes at the scale of the crystal lattice. A number of useful texts have been written on the subject including Hill (1950), Kachanov (1971), and Lubliner (1990). Plastic deformation in metals is observed to be *isochoric*, or volume preserving. It follows that the deviatoric stress is responsible for driving plastic flow in metals, since it does not cause a volume change. Classical  $J_2$  flow theory is named for its explicit relation to the second

invariant of the deviatoric stress.

Computationally, the increased availability of computing resources and development of the finite element method for nonlinear problems allowed for the parallel development of the computational formulation of plasticity. Standard texts for the finite element method include Hughes (1987) and Zienkiewicz and Taylor (1989). Of utmost importance was the development of numerical integration schemes for classical plasticity, such as early work based on the radial return algorithm for perfect plasticity presented in Wilkins (1963). Extensions for hardening and finite strain for the radial return algorithm came in Krieg and Key (1976) and Key and Krieg (1982). Significant generalization of those ideas were presented in Ortiz and Simo (1986), Simo (1988a), Simo (1988b), and Simo (1992) where *return mapping* algorithms were introduced and analyzed in the context of hyperelasticity, multiplicative plasticity, and non-associative flow laws. Comprehensive references for the formulation and implementation of integration algorithms for inelastic constitutive equations can be found in Simo (1998) and Simo and Hughes (1998).

*Gradient plasticity* builds upon the classical theory of plasticity by introducing fields within the constitutive theory that are themselves, in some manner, gradients of strains. The motivation behind these additions are the inability of the classical theory to account for such phenomena as *size effects* and *softening* pathologies. Size effects are observed as a dependence of the plastic flow stress on a characteristic dimension of the specimen. Softening is an observed decrease in strength of a material for a given strain increment. Softening produces pathological mesh dependent behavior, which is a manifestation of the non-uniqueness of the solution when softening moduli are present, as the boundary value problem is ill-posed. Treatments for size effects and softening can come from adding a length scale to the continuum formulation, as in a gradient theory, or via numerical treatments, for example in a nonlocal damage theory.

In Coleman and Hodgdon (1985) the authors are motivated by the observations of adiabatic shear bands in metals and the softening of geological materials due to the accumulation of damage. In an analysis of shear bands, they propose including a term that accounts for the spatial derivative of the accumulated shear strain in the evaluation of the stress field. In the generalization to three dimensions, the term becomes the Laplacian of the (scalar) accumulated distortion. It should be noted that the authors make a point of proclaiming the model is constructed to produce solutions similar to the observed behavior of some materials, and not motivated by first principles.

Aifantis undertakes a physically motivated exploration of dislocation phenomena, including the transition from micro-scale behaviors to the macro-scale, physically based finite deformation continuum theories, and applications of the theory to localization problems (Aifantis, 1987). The author introduces second gradients of the (scalar) equivalent plastic strain, similar to the work of Coleman and Hodgdon, that serve to regularize the solution of softening boundary value problems. In Muhlhaus and Aifantis (1991), a variational statement is presented that incorporates the Laplacian of the plastic consistency parameter. The weak form of the statement then requires the same interpolation functions for both the displacements and the plastic parameter, but introduces the need for boundary conditions

related to the plastic fields.

The authors in Fleck and Hutchinson (1993) and Fleck et al. (1994) attempt a physical derivation of a gradient plasticity model with the intention of predicting size effects in materials. Motivated by a description of geometrically necessary dislocations in areas of a body with a gradient in strain, they incorporate the Cosserat couple stress theory to construct a constitutive model that depends both on the strain and the gradient of the strain. The model accounts for the accumulation of geometrically necessary dislocations in areas of intense strain gradients, and the authors use the model to explain observations of gradient dependent hardening in a series of torsion tests on wire with diameters ranging from 12 to 170  $\mu\text{m}$ .

In Nix and Gao (1998), Gao et al. (1999), and Huang et al. (2000) the authors propose a theory of mechanism based strain gradient plasticity. The authors are motivated to resolve the observation in indentation experiments that the hardening response for a material increases as the size of the indenter decreases. The presumably occurs due to the strong gradient in the localization zone adjacent to the indenter. Again, the authors aim to account for the effective density of geometrically necessary dislocations that arise due to strong gradients. To accomplish this they introduce the concept of a dislocation density tensor, which is then used in the construction of the (continuum) theory.

In Cermelli and Gurtin (2001) the authors formally develop the notion of the Burger's tensor, including a thorough review of the many forms a dislocation based tensor has taken in the literature. Using that concept Gurtin (2004) and Gurtin (2005) employ a *micro force balance* to derive balance laws for plastically deforming materials that account for gradient effects via the dislocation tensor. It is upon these theories that the model presented in this dissertation will be built.

Other approaches for introducing length scales, motivated by localization phenomena in geological materials, are the *nonlocal* theories, where spatial dependence of the local quantities is achieved via sampling fields within a finite radius. Typically the nonlocal theories are concerned with the spatial dependence of damage, or the accumulated degradation of a material with strain, as in Bazant et al. (1984) and Bazant and Pijaudier-Cabot (1988). The length scale that is introduced is essentially the radius by which the damage field is integrated within, as the integration of damage dictates the width of shear bands in softening materials.

Experiments have been conducted with the expectation that at small enough scales, the micromechanics provided by dislocation theory will dominate the behavior. Notably, in Fleck and Hutchinson (1993) microtorsion experiments are presented and compared with microtension experiments. The torsion experiments exhibit a marked dependence on the diameter of the copper wire, indicating a strong constitutive dependence on the gradient of the strain, while the tension experiments show an insignificant dependence on wire diameter. In Stölken and Evans (1998) the authors develop a microbending test to determine the gradient dependence of very thin foils of high purity nickel. The test method measures the deformed radius of curvature of an elastically unloaded foil. The results show that for a

given surface strain, the applied bending moment increased noticeably as the thickness of the foil decreased, giving further credence to the notion of a size effect for plasticity at small scales. In Ma and Clarke (1995) the authors show that measured hardness for silver single crystals is also dependent on the size of the indentation. As the indenter sized decreased, especially below 10  $\mu\text{m}$ , the measured hardness increased.

Each of the preceding gradient plasticity theories includes higher order terms associated with the newly introduced gradient dependence. For example, the theory from Fleck and Hutchinson includes a third-order stress term when the displacements are the only primal fields. Gurtin presents a model where an additional second-order stress term is included. With the introduction of higher order gradients within weak form of the plastic constitutive theory, usually in the form of partial differential equations, higher-order boundary conditions become necessary. Physically based notions of these boundary conditions have remained elusive, and in many cases are not discussed beyond the acknowledgement that they exist. More stringent continuity requirements also arise directly from the additional spatial derivatives found in gradient theories, specifically to address the additional boundary conditions. Additional requirements limit or eliminate the use of classical numerical techniques for these higher-order theories.

The solution of higher-order theories by the finite element method involves employing some mechanism of achieving higher-order continuity of the basis functions in the weak form. In particular, for fourth order theories assuming a displacement based formulation, after repeated integration by parts, continuity requirements dictate that the solution basis functions be  $\mathcal{C}^1$ , which means that both the solution and its first derivative are continuous. Constructing  $\mathcal{C}^1$  continuous basis functions in three dimensions is reported as anything from very complicated to intractable in the literature. An alternative approach is the introduction of another field, usually representative of the gradient of the original field, which allows the relaxation of the continuity requirements. Again, for a fourth-order theory each field would need  $\mathcal{C}^0$  continuity. These *mixed methods*, unfortunately inherit additional stability requirements. As pointed out in Brezzi (1990), applicability of mixed methods is determined via mathematical analysis, which is generally a non-trivial task. Furthermore, stability will depend on the specific interpolations chosen for each field, with the unsettling result that some combinations of basis functions work, while others do not.

*Discontinuous Galerkin* (DG) methods are formulations in which the weak form is written to include integrals across inter-element interfaces. In the context of elliptic problems the fluxes that appear across the interfaces are approximated by so-called *numerical fluxes*. These numerical fluxes can be used to capture discontinuities in fields or manipulated in other ways to approximate derivatives in a distributional sense, in effect achieving an approximation of greater continuity. DG methods started appearing in the literature in the early 1970s. Reed and Hill (1973) developed a DG method to solve the hyperbolic neutron transport equations, but the methods were also being developed for elliptic problems. Nitsche (1971) proposed an early symmetric and consistent method for elliptic problems that used an *interior penalty*, and more recently Bassi and Rebay (1997) applied DG methods to the Navier-Stokes equations by introducing a term later denoted as the *lifting operator*.

Arnold et al. (2002) presented a unifying analysis of methods for elliptic problems.

Discontinuous Galerkin methods have become attractive in view of the difficulties associated with higher-order partial differential or differential-algebraic equations, including the need for  $\mathcal{C}^1$ -continuous elements. Discontinuous Galerkin based  $\mathcal{C}^0$  finite element basis functions were developed for fourth-order elliptic problems related to thin beam and plate theory and gradient elasticity in Engel et al. (2002). The proposed methods used concepts from both the continuous and discontinuous Galerkin as well as stabilization techniques where low-order polynomials were used and continuity requirements were weakly enforced via stabilization of interior facet terms. Wells et al. (2004) and Molari et al. (2006) discuss strain gradient damage. The fourth-order Cahn-Hilliard equation for phase segregation gets a treatment in Wells et al. (2006). DG formulations for Kirchoff-Love plates and shells are presented in Wells and Dung (2007) and Noels and Radovitzky (2008). Djoko et al. (2007a), Djoko et al. (2007b) and McBride (2008) present a DG formulation for a gradient plasticity model similar to that of Aifantis.

## 1.2 An Overview

Chapter 2 has an introduction to dislocations and a discussion of the role dislocation motion plays in plastic deformation. Crystal structure and slip systems are introduced as precursors to the notion of a dislocation. Edge and screw dislocations are discussed, and an example of dislocation motion is presented. Hardening mechanisms related to the generation and interaction of dislocations are also presented. Then, leading up to a gradient plasticity constitutive theory, the discrete notion of incompatibility in a crystal lattice, or the Burger's vector, is manipulated to arrive at a continuum, tensorial quantity called the Burger's tensor.

Chapter 3 uses the continuum concepts of Burger's vector presented in Chapter 2 and constructs a constitutive model with a gradient dependence on the plastic part of the displacement gradient. A free energy is chosen to incorporate conjugate pairs for the elastic and plastic displacement gradients, as well as the curl of the plastic part of the displacement gradient. A microforce balance is then used to derive a pair of partial differential equations that govern the macroscopic balance of momenta, or equilibrium, and the microscopic balance of forces that can be interpreted as the flow rule for the plasticity model.

In Chapter 4 applicability of the DG method for gradient plasticity is stated, followed by a derivation of the variational statement of the coupled set of partial differential equations derived in Chapter 3. DG methods are used to weakly enforce the necessary continuity requirements of the plastic fields.

An algorithm describing the implementation of the variational form into a nonlinear finite element code is presented and discussed in Chapter 5. Specifically, there is a discussion of the mixed plasticity formulation that serves as the foundation for the gradient model implementation. Then the choice of interpolation space for the plastic variables is discussed.

Chapter 6 provides numerical results using the implementation of the variational formulation of gradient plasticity presented here. The mixed formulation for plasticity is verified. Further, some selected results using a constant basis for the plastic distortion are presented, as well as current efforts to solve the equations using a linear basis.

Chapter 7 consists of conclusions and final comments. Model strengths and weaknesses are discussed, including a brief discussion on the need for additional experimental results, as well as possible future directions for both the gradient plasticity model and DG methods.

# Chapter 2

## Dislocation Based Plasticity

This chapter is devoted to an elementary discussion of dislocation theory in the context of describing plastic deformation, and the extension of these ideas into a continuum treatment. Dislocation theory provides some insight into the micro-mechanical behavior of single and polycrystalline materials. In particular, the origins of dislocation theory are concerned with metals, which are indeed polycrystalline. Dislocation theory, however, does not provide a definitive model of plastic behavior at the macro scale, the reason being that interactions between dislocations and their surrounding environments, which may include obstacles such as grain boundaries or even other dislocations, are far too numerous and complex to be efficiently modeled. All encompassing theory lacking, some aspects of plastic deformation can be described quite well by dislocation theory and for that reason, and the fact that the generally accepted mechanism for plastic flow is dislocation motion, it is worth taking the time to understand.

### 2.1 Plasticity in Crystals

A crystal is a solid formed by a three-dimensional pattern of repeating atoms which form a lattice. For metals, there are three particular patterns which occur most often, hexagonal close packed (HCP), face centered cubic (FCC), and body centered cubic (BCC). Figure 2.1 shows examples of each of these crystal structures, and Table 2.1 gives examples for each crystal structure. The notion of *slip* embodies the idea of the relative motion between atoms. The lattice structure, or pattern, gives rise to two crystallographic quantities, slip planes and slip directions. Slip planes are planes which are parallel to the planes of atoms which have the closest packing distance. The closest packing distance is the direction in which the distance between atoms is the smallest. Within a slip plane, directions parallel to the closest packing distance are called slip directions. Together for a given crystal, slip planes and slip directions are known as *slip systems*. It is observed experimentally that plastic deformation is the result of the slip, or relative atomic motion, along slip planes under a given shear stress.

One method for determining the shear stress necessary to achieve slip along the favorable crystallographic directions is known as Schmid's law. Consider a single crystal tensile specimen under a stress  $\sigma$  along its axis, which forms an angle  $\phi$  with the normal of a slip plane, and

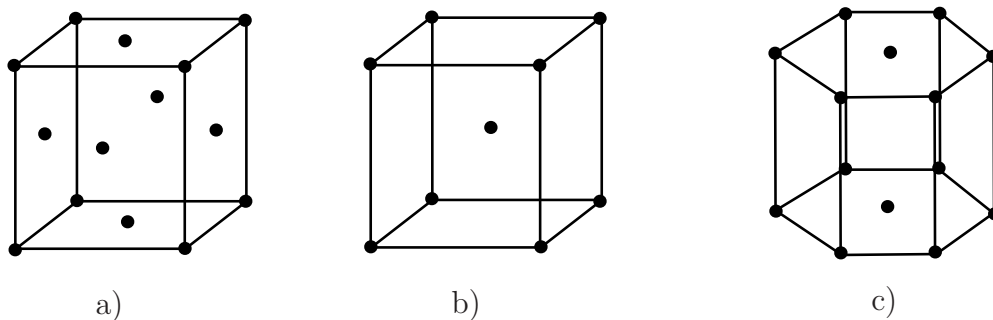


**Figure 2.1.** Common metal crystals: a) FCC, b) BCC, c) HCP

Crystal Structure	Metal
FCC	Aluminum, Copper, Gold
BCC	$\alpha$ -Iron, Tungsten
HCP	Zinc, Magnesium

**Table 2.1.** Examples of FCC, BCC, and HCP metals

another angle  $\lambda$  with the slip direction. The shear stress resolved along the slip plane that produces plastic deformation, known as the critically resolved shear stress, can be seen in (2.1). For a schematic depiction of the process, see Figure 2.2.

$$\tau_c = \cos\phi \cos\lambda \sigma \quad (2.1)$$

If we consider that slip is the primary mechanism for plastic deformation, then it is plausible to determine the shear stress necessary to displace one plane of atoms over another. The result is the theoretical shear strength of a material. To calculate a simple approximation, assume the stress necessary to move the top plane of atoms in Figure 2.3 is periodic. This assumption is justified by noting that if the lattice is initially in equilibrium, then a displacement of  $x = b$  will return it to equilibrium, and a displacement of  $x = b/2$  would place it in an unstable equilibrium.

$$\tau = \tau_{max} \sin \frac{2\pi x}{b} \quad (2.2)$$

Now to first-order,  $\tau = 2\pi\tau_{max}x/b$ , and for a small displacement,  $x$ , we know from elasticity that  $\tau = G\gamma$ , where the shear strain  $\gamma = x/a$ . It follows that

$$\tau_{max} = \frac{Gb}{2\pi a}. \quad (2.3)$$

Observe that in (2.3), the theoretical shear strength of a material is within an order of magnitude of the shear modulus  $G$  if  $b$  is close to  $a$ . The startling observation that prompted

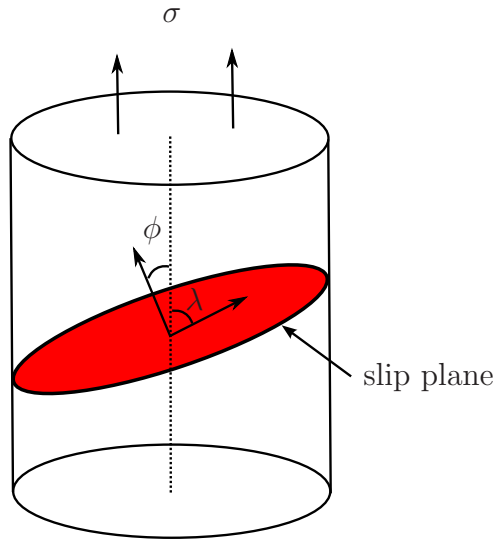


**Figure 2.2.** Slip plane in a body under uniaxial tension

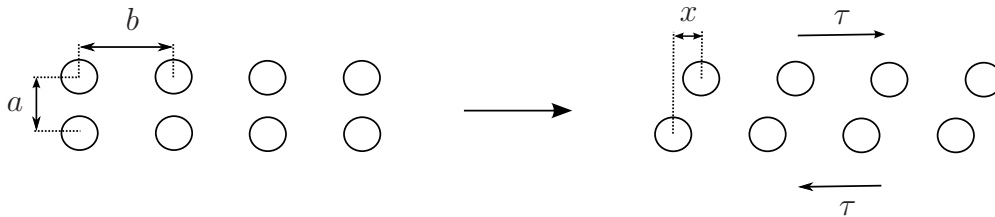


**Figure 2.3.** Relative displacement of a whole plane of atoms

development of the theory of dislocations was that actual measurements of the shear strength of single crystals are *three to five orders of magnitude less* than the shear modulus. Obviously, the mechanism for plastic deformation was not whole planes of atoms in relative motion.

To resolve the discrepancy between the theoretical shear strength and measured values the concept of dislocations as specific defects in the lattice was proposed by both G.I. Taylor and E. Orowan circa 1934, for reference see the work by Taylor Taylor (1938). The basic idea proposes dislocations as line defects in a lattice, or a line of vacancies, which then permit the relative motion of only a few atoms to achieve slip. This theory sufficiently accounts for observed shear strengths, as will be seen below. Two basic types of dislocations exist: edge and screw. Edge dislocations can be thought of as arising from inserting an extra plane of atoms into an existing crystal. At the termination of the extra plane the lattice becomes distorted. The imperfection in the distorted lattice can be characterized by the lack of closure of a loop, or *Burger's circuit*, through the unperturbed lattice around the imperfection. This characterization is referred to as the Burger's vector, and can be thought of as a measure of

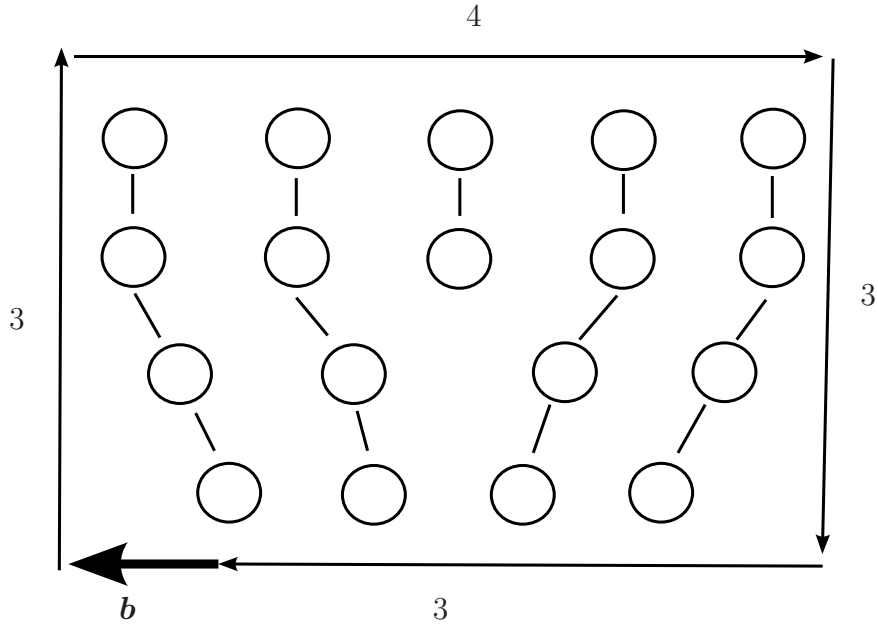


**Figure 2.4.** An edge dislocation with Burger's vector,  $\mathbf{b}$

the *incompatibility* of the lattice. For an illustration of the Burger's vector,  $\mathbf{b}$ ,<sup>1</sup> for an edge dislocation, see Figure 2.4. Note that the dislocation line, recalling that dislocations are line defects, would continue in and out of the page from the point of imperfection, and that the dislocation line is perpendicular to the Burger's vector for an edge dislocation. A screw dislocation, as can be seen in the three dimensional schematic in Figure 2.5, can be thought of as making a partial cut through a lattice, and then displacing the cut portions in a shear direction until the lattice lines up again. A significant distinction between edge and screw dislocations is the fact that while edge dislocations have  $\mathbf{b}$  perpendicular to the dislocation line, screw dislocations have  $\mathbf{b}$  parallel to the dislocation line. In reality, dislocations may be of mixed character, meaning that a portion of the dislocation has edge character, and a portion has screw character. However, the Burger's vector is conserved.

To make concrete the connection between plasticity and dislocations, consider a lattice with a dislocation present under an applied shear stress. When the stress reaches a critical value, it becomes energetically favorable for bonds between atoms to switch, effectively transporting the dislocation through the lattice. This *dislocation motion* is the primary mechanism for plastic deformation in crystalline materials. It is worth pointing out that while the presence of a dislocation within a crystal lattice induces a local elastic stress field, plastic deformation is not realized until a sufficient applied stress causes that dislocation to move. A simple schematic of an edge dislocation progressing through a lattice under an applied shear stress,  $\tau$ , can be seen in Figure 2.6.

<sup>1</sup>Not to be confused with a body force, which should subsequently be clear from the context.

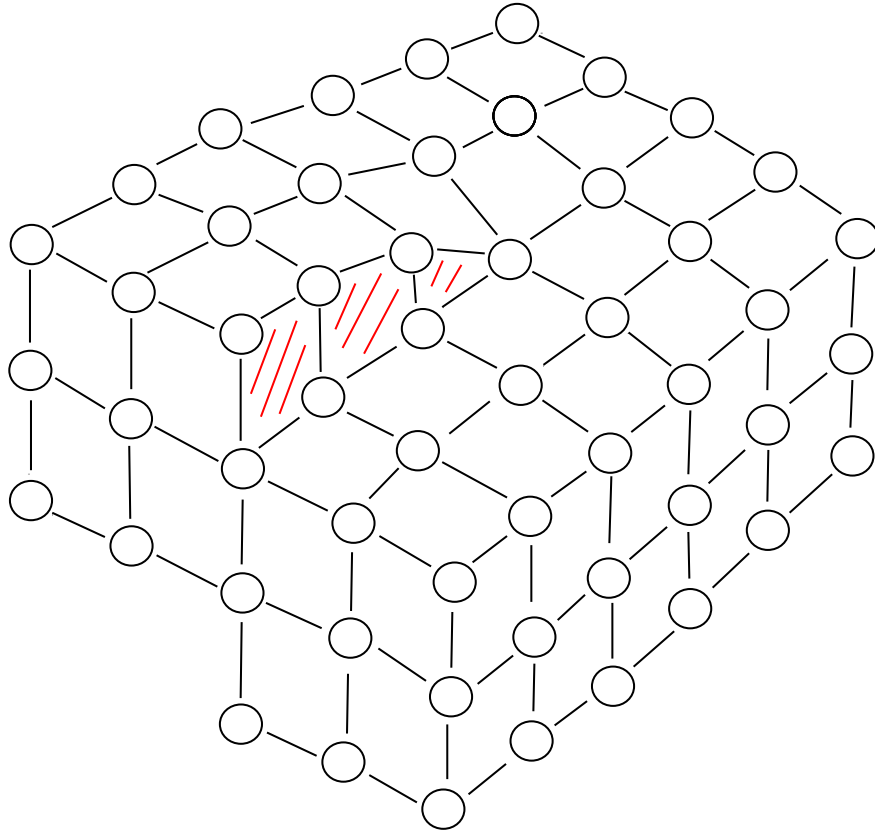


**Figure 2.5.** A screw dislocation

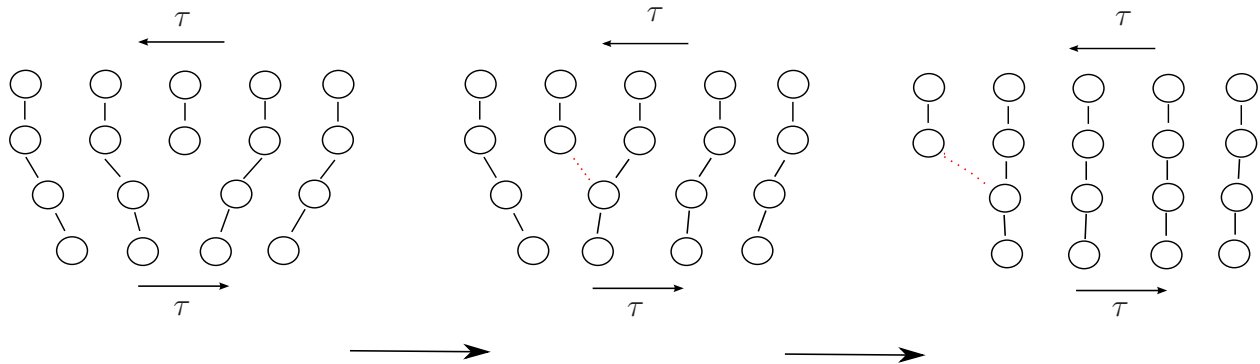


**Figure 2.6.** Edge dislocation moving through a lattice

A better approximation for the applied stress necessary to produce dislocation motion than the theoretical shear strength (2.3) is given by the Peirls-Nabarro stress.

$$\tau_{PN} = \frac{2G}{1-\nu} \exp\left(\frac{-2\pi h}{d(1-\nu)}\right) \quad (2.4)$$

In (2.4),  $h$  denotes the distance between adjacent planes of atoms,  $d$  denotes the distance between atoms in each plane,  $G$  is the shear modulus, and  $\nu$  is Poisson's ratio. The first notable observation from (2.4) is that the predicted critical shear stress is on the order of experimental observations for single crystals. Second, as the ratio  $h/d$  increases,  $\tau_{PN}$  decreases, which corresponds to more densely packed planes and/or larger separation between close packed planes, which is consistent with the notion of slip systems playing an important role in a material's plastic behavior.

Dislocation theory can also be applied to explain how a material work hardens under an applied load. The notion of hardening at the micro-structural level can be expressed as the increased load necessary to continue to move a dislocation through a lattice when it has encountered an obstacle. This increased load manifests as hardening in a macroscopic load displacement curve. Consider a polycrystalline aggregate, such as a metal, comprised of multiple grains at different orientations. Then the crystal structure is generally not continuous across grain boundaries. Consider also that within each grain the crystal structure is likely imperfect and contains dislocations of various character. Now consider an applied load sufficient in magnitude to produce dislocation motion. Taking an elementary view yields two observations. First, as dislocations move within a crystal grain, they will encounter other dislocations that will serve as obstacles, increasing the stress necessary to propagate them further. Second, grain boundaries will also act to impede the motion of dislocations, again increasing the applied load necessary to produce dislocation motion. These are two of the simplest examples of hardening in a polycrystalline material.

An explanation for the Bauschinger effect comes from the idea that dislocations tend to pile-up at grain boundaries. To further this notion, the idea of *dislocation annihilation* needs to be introduced. Imagine another edge dislocation, similar to Figure 2.4, except that the extra plane of atoms is inserted from the bottom of the lattice instead of from the top. These two dislocations would have opposite *sign*. It follows that when two dislocations of opposite sign interact, the net result is dislocation annihilation, leaving the lattice unperturbed. Another point to make is that dislocations of the same sign have stress fields that tend to repulse one another. With these two concepts stated, the Bauschinger effect can be explained as follows in two parts. First, upon loading dislocations of like sign pile up at grain boundaries, creating a back stress due to the same sign repulsion. Upon unloading, the repulsion aids in dislocation motion in the reverse direction, effectively reducing the yield strength. The second part to the explanation assumes that dislocations of the opposite sign are produced when the loading is reversed, and the interaction of the new dislocations with those already existing causes annihilation, reducing the total number of potential obstacles and the yield strength in the process.

It is left to describe how dislocations are produced within a crystal in order to explain both the second explanation of the Bauschinger effect, and the fact that some materials

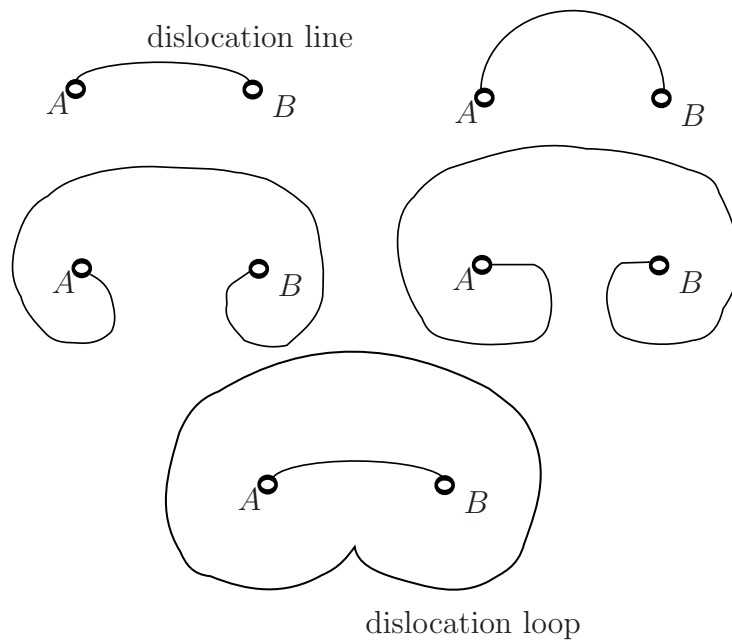


**Figure 2.7.** A Frank-Read source for dislocation generation

can achieve extremely high levels of plastic deformation. For the latter, if the dislocation number was fixed from the initial state, a material would be limited in the amount of plastic deformation it could experience by the number of dislocations it has, which is not the case. One such explanation for dislocation generation is known as a Frank-Read source. To begin, consider a dislocation line, fixed at the nodes *A* and *B*, subject to an applied load. The obstacles preventing the motion of the dislocations at *A* and *B* are not important for this description, but could be point defects or other obstacles that render the dislocation immobile at those points. Under the applied load, the dislocation line will bulge out in the direction of the stress, and will eventually reach a critical point where it will spiral around the pinning points. When the dislocation loop meets with itself, it annihilates creating a complete dislocation loop and a new dislocation line between the pinning points, *A* and *B*. For a visual depiction of the Frank-Read source, refer to Figure 2.7. Other dislocation generation mechanisms exist as well, such as multiple cross slip, which will not be discussed here.

The ideas presented above represent just an elementary view of the science of dislocations. Concepts such as temperature dependence, dislocation glide and climb, velocity and density have been omitted from this discussion. It should be clear that dislocation motion is capable of describing plasticity and hardening mechanisms in single crystals and polycrystalline aggregates. Lacking is an efficient and general bridge between the micro-mechanical behaviors and the macro-scale continuum theories of plasticity. Subsequent developments in this document will attempt to address this issue, presenting an incompatibility based hardening mechanism within the context of a continuum theory.

## 2.2 Extending Burger's Vector to the Continuum

The objective of this section is to use the concept of the Burger's vector,  $\mathbf{b}$ , introduced above and develop a continuum measure of incompatibility. The continuum quantity that can be related to a measure of the incompatibility in a lattice is termed the *Burger's tensor*, and is denoted by  $\mathbf{G}$ . The concept of the Burger's tensor has been extensively studied, for background see Cermelli and Gurtin (2001) and references within. Modern treatments begin in the general setting with the multiplicative decomposition of the deformation gradient into elastic and plastic parts, as in (2.5), due largely to Lee (1969) and Kroner and Teodosiu (1972).

$$\mathbf{F} = \mathbf{F}^e \mathbf{F}^p \quad (2.5)$$

Note that in the context of finite deformation the additive decomposition no longer holds in general, but can be recovered from the general theory under certain small strain assumptions. The physical significance of (2.5) in the context of crystal plasticity can be found in Asaro (1983), where the plastic part of the deformation gradient,  $\mathbf{F}^p$ , is due solely to the plastic slip along the slip planes of the lattice in question.

Using the multiplicative decomposition, various definitions of  $\mathbf{G}$  are compared and contrasted in Cermelli and Gurtin (2001). The main objective of the remainder of this section will be to derive a  $\mathbf{G}$  suitable for formulating a small strain continuum constitutive theory, and for this reason the following material will follow closely with the work in Gurtin (2004). We can restrict the theory to the small strain context pertinent to this dissertation by recalling a particular definition of the deformation gradient. Then the small strain version of the multiplicative decomposition of the deformation gradient becomes the additive decomposition of the displacement gradient as in (2.6).

$$\nabla \mathbf{u} = \mathbf{H}^e + \mathbf{H}^p \quad (2.6)$$

Here,  $\mathbf{H}^e$  is now the elastic part of the displacement gradient, and  $\mathbf{H}^p$  is the plastic part of the displacement gradient. As plastic deformation is observed to be isochoric, an additional restriction is placed on the plastic part of the displacement gradient, or plastic distortion, namely  $\text{tr } \mathbf{H}^p = 0$ . The insistence that  $\mathbf{H}^p$  be deviatoric is similar to the construction of  $\boldsymbol{\varepsilon}^p$  as deviatoric in the classical theory. A pertinent feature of the theory is that there is no assumption, *a priori*, that the plastic spin,  $\boldsymbol{\omega}^p = \text{skew } \mathbf{H}^p$ ,<sup>2</sup> provides no contribution to the free energy of the plastically deformed body as in the classical theory. In fact, assuming zero plastic spin is the simplest possible assumption to recover the additive decomposition of strain in the classical theory, because the classical theory only deals with strains, which are the symmetric part of the displacement gradients. The inclusion of the plastic spin occurs as a natural consequence of the characterization of the Burger's tensor in a continuum body. A measure of the incompatibility in the plastic distortion,  $\mathbf{H}^p$ , can be related to the Burger's vector via Stokes' theorem, which integrates an infinitesimal loop, similar to the Burger's

---

<sup>2</sup>Recall the Euclidean decomposition of a second rank tensor,  $\mathbf{T}$ , into its symmetric and skew symmetric parts,  $T_{ij} = S_{ij} + W_{ij}$ , where  $S_{ij} = S_{ji}$  and  $W_{ij} = -W_{ji}$ . Then we say the  $\mathbf{H}^p$  can be decomposed into the plastic strain and plastic spin as  $\mathbf{H}^p = \boldsymbol{\varepsilon}^p + \boldsymbol{\omega}^p$ .

circuit mentioned above. In the small strain setting where configuration mapping terms can be neglected, for a smooth oriented surface,  $S$  with boundary  $\partial S$

$$\oint_{\partial S} \mathbf{H}^p \, d\mathbf{X} = \int_S (\text{curl } \mathbf{H}^p)^\top \mathbf{n} \, dA, \quad (2.7)$$

where  $\mathbf{n}$  is the unit normal to the surface  $S$ . Then the definition of the Burger's tensor follows as

$$\mathbf{G} = \text{curl } \mathbf{H}^p. \quad (2.8)$$

The quantity  $\mathbf{G}^\top \mathbf{n}$  gives a measure of the Burger's vector, per unit area, for a plane with unit normal,  $\mathbf{n}$ . It is worth noting that for a theory to properly capture the effects of the Burger's tensor, the evolution of the plastic spin must be accounted for, since  $\mathbf{H}^p = \boldsymbol{\varepsilon}^p + \boldsymbol{\omega}^p$ , and  $\mathbf{G} = \text{curl } \mathbf{H}^p$ . It follows that classical methods, which do not have any notion of plastic spin, are not equipped to deal with the notion of the Burger's vector correctly.

The Burger's vector, per unit area,  $\mathbf{G}^\top \mathbf{n}$ , can be thought of as evolving according to a balance. Consider the time rate of change,

$$\overline{\mathbf{G}^\top \mathbf{n}} = (\text{curl } \dot{\mathbf{H}}^p)^\top \mathbf{n} = -\text{div} (-\dot{\mathbf{H}}^p(\mathbf{n} \times)), \quad (2.9)$$

where  $(\mathbf{n} \times)$  is the skew tensor  $(\mathbf{n} \times)_{ij} = \varepsilon_{irj} n_r$ , and  $\dot{\mathbf{H}}^p(\mathbf{n} \times)$  represents a tensorial Burger's vector flux through planes with normal  $\mathbf{n}$ . As a result of this balance, we have the following result,

$$\dot{\mathbf{H}}^p(\mathbf{n} \times) = 0, \quad (2.10)$$

which holds at a particular point if and only if there is no Burger's vector flow across the plane with unit normal  $\mathbf{n}$ .



# Chapter 3

## Gradient Plasticity Model

To begin the development of the gradient dependent constitutive model, recall the additive decomposition of the displacement gradient into elastic and plastic parts.

$$\nabla \mathbf{u} = \mathbf{H}^e + \mathbf{H}^p \quad (3.1)$$

Also recall that  $\text{tr } \mathbf{H}^p = 0$ , indicating the deviatoric nature of the plastic distortion. A priority in development of the theory is a mechanism by which to account for the Burger's vector and Burger's vector flux, and so the theory will depend on the definition of the Burger's tensor,

$$\mathbf{G} = \text{curl } \mathbf{H}^p. \quad (3.2)$$

The principal of virtual power will be employed to derive the macroscopic balance of momenta, and what Gurtin terms the microforce balance, by which we will determine the flow rule. In order to achieve a theory that accounts for incompatibilities, two stresses are introduced,  $\mathbf{T}^p$  and  $\mathbb{S}$ , conjugate to  $\mathbf{H}^p$  and  $\mathbf{G}$  respectively. Then we can define the internal power as

$$\mathcal{W}_{int} = \int_{\Omega} \boldsymbol{\sigma} : \dot{\mathbf{H}}^e + \mathbf{T}^p : \dot{\mathbf{H}}^p + \mathbb{S} : \dot{\mathbf{G}} \, dV \quad (3.3)$$

where  $\boldsymbol{\sigma}$  is the Cauchy stress,  $\mathbf{T}^p$  is termed the microstress which has deviatoric nature like  $\mathbf{H}^p$  ( $\text{tr } \mathbf{T}^p = 0$ ), and  $\mathbb{S}$  is termed the defect stress. Next, the external power can be defined as

$$\mathcal{W}_{ext} = \int_{\Omega} \mathbf{b} \cdot \dot{\mathbf{u}} \, dV + \int_{\partial\Omega} \mathbf{S}(\mathbf{n}) : \dot{\mathbf{H}}^p + \mathbf{t}(\mathbf{n}) \cdot \dot{\mathbf{u}} \, dS, \quad (3.4)$$

where  $\mathbf{b}$  is now the body force (not to be confused with the Burger's vector which henceforth will not be explicitly mentioned),  $\mathbf{t}(\mathbf{n})$  is a macroscopic traction, and  $\mathbf{S}(\mathbf{n})$  is a microtraction related to the flow of dislocations across surfaces. All stress and stress-like quantities are assumed to be invariant under superposed rigid rotations.

Using the expressions in 3.3 and 3.4, we denote a set of virtual velocities,  $\mathcal{V} = (\mathbf{w}, \mathbf{v}, \mathbf{V})$  corresponding to  $\dot{\mathbf{u}}$ ,  $\dot{\mathbf{H}}^e$ , and  $\dot{\mathbf{H}}^p$ . The following requirements are placed on the virtual velocities, consistent with their non-virtual counterparts.

$$\nabla \mathbf{w} = \mathbf{v} + \mathbf{V} \quad (3.5)$$

$$\text{tr}(\mathbf{V}) = 0 \quad (3.6)$$

It is assumed that the virtual velocities transform under superposed rigid rotations in a similar manner as the quantities from which they are derived, which gives  $\mathbf{v} \rightarrow \mathbf{v} + \mathbf{W}$  for a rigid rotation,  $\mathbf{W}$ , while  $\mathbf{V}$  and  $\text{curl } \mathbf{V}$  are invariant. We arrive at the virtual internal and external power by inserting the relevant virtual terms into 3.3 and 3.4.

$$\mathcal{W}_{int}(\mathcal{V}) = \int_{\Omega} \boldsymbol{\sigma} : \mathbf{v} + \mathbf{T}^p : \mathbf{V} + \mathbb{S} : \text{curl } \mathbf{V} \, dV \quad (3.7)$$

$$\mathcal{W}_{ext}(\mathcal{V}) = \int_{\Omega} \mathbf{b} \cdot \mathbf{w} \, dV + \int_{\partial\Omega} \mathbf{S}(\mathbf{n}) : \mathbf{V} + \mathbf{t}(\mathbf{n}) \cdot \mathbf{w} \, dS \quad (3.8)$$

The principal of virtual power can then be stated as a balance between virtual internal and external power, and frame indifference of the internal virtual power.

$$\mathcal{W}_{int}(\mathcal{V}) = \mathcal{W}_{ext}(\mathcal{V}) \quad (3.9)$$

Next, the classical macroscopic momentum balances will be stated, as in Gurtin (2004).

$$\text{div } \boldsymbol{\sigma} + \mathbf{b} = \mathbf{0} \quad (3.10)$$

$$\mathbf{t}(\mathbf{n}) = \boldsymbol{\sigma} \mathbf{n} \quad (3.11)$$

The flow rule for this theory comes from a microforce balance. The microforce balance can be thought of as the microscopic counterpart of the macroscopic balances. To that end we introduce an identity that is essentially the integration by parts of one of the terms in the virtual internal power. For tensor fields  $\mathbf{A}$  and  $\mathbf{B}$ ,

$$- \int_{\partial\Omega} (\mathbf{n} \times \mathbf{A}) : \mathbf{B}^T \, dS = \int_{\Omega} (\mathbf{A} : \text{curl } \mathbf{B} - \mathbf{B}^T : \text{curl } (\mathbf{A}^T)) \, dV. \quad (3.12)$$

The tensor  $\mathbf{n} \times$  is the skew object with axial vector  $\mathbf{n}$ . This becomes a useful way to restate the first term in 3.12. Moving on, we choose a virtual velocity  $\mathbf{w} = 0$ , so that  $\mathbf{v} = -\mathbf{V}$ , and we then write the associated virtual power relation from 3.9, again using 3.7 and 3.8.

$$\int_{\partial\Omega} \mathbf{S}(\mathbf{n}) : \mathbf{V} \, dS = \int_{\Omega} ((\mathbf{T}^p - \boldsymbol{\sigma}) : \mathbf{V} + \mathbb{S} : \text{curl } \mathbf{V}) \, dV \quad (3.13)$$

Now we use 3.12 to obtain

$$\int_{\partial\Omega} (\mathbf{S}(\mathbf{n}) + ((\mathbf{n} \times) \mathbb{S})^T) : \mathbf{V} \, dS = \int_{\Omega} ((\mathbf{T}^p - \boldsymbol{\sigma} + (\text{curl } (\mathbb{S}^T))^T) : \mathbf{V}) \, dV. \quad (3.14)$$

From this we deduce the microforce balance using the fact that  $\mathbf{V}$  is deviatoric and  $\boldsymbol{\sigma}$  is symmetric.

$$\mathbf{s} = \mathbf{T}^p + (\text{dev } \text{curl } (\mathbb{S}^T))^T \quad (3.15)$$

Where  $\mathbf{s}^1$  is the deviatoric part of the Cauchy stress. Similarly, we arrive at the microtraction condition using the fact that for the skew tensor  $(\mathbf{n} \times)^T = -(\mathbf{n} \times)$ .

$$\mathbf{S}(\mathbf{n}) = \text{dev } (\mathbb{S}^T (\mathbf{n} \times)) \quad (3.16)$$

---

<sup>1</sup>Care must be taken to distinguish between the deviatoric part of the Cauchy stress,  $\mathbf{s}$ , the defect stress,  $\mathbb{S}$ , and the microtraction,  $\mathbf{S}(\mathbf{n})$ .

To complete the model we need to develop constitutive expressions for the various stresses. In formulating the constitutive theory, a free energy is chosen of the form  $\Psi(\boldsymbol{\varepsilon}^e, \mathbf{G})$ , and the macro and micro stresses are defined to be thermodynamically conjugate to the kinematic tensors  $\boldsymbol{\varepsilon}^e$  and  $\mathbf{G}$ , respectively. The elastic free energy is defined in the standard way as  $\Psi^e(\boldsymbol{\varepsilon}^e) = \frac{1}{2}\boldsymbol{\varepsilon}^e : \mathbb{C} : \boldsymbol{\varepsilon}^e$ , such that the usual definition of stress results,  $\boldsymbol{\sigma} = \mathbb{C} : \boldsymbol{\varepsilon}^e$ .

$$\Psi(\boldsymbol{\varepsilon}^e, \mathbf{G}) = \Psi^e(\boldsymbol{\varepsilon}^e) + \frac{1}{2}k|\mathbf{G}|^2 \quad (3.17)$$

$$\boldsymbol{\sigma} = \frac{\partial \Psi}{\partial \boldsymbol{\varepsilon}^e} = \mathbb{C} : \boldsymbol{\varepsilon}^e \quad (3.18)$$

$$\mathbb{S} = \frac{\partial \Psi}{\partial \mathbf{G}} = k \mathbf{G} = k \operatorname{curl} \mathbf{H}^p \quad (3.19)$$

Taking the symmetric part of the additive decomposition of the displacement gradient, 2.6, we get an expression for the total strain,  $\boldsymbol{\varepsilon} = \boldsymbol{\varepsilon}^e + \boldsymbol{\varepsilon}^p$ . From this we can deduce an expression for the elastic strain, and thus recover the classical definition of the Cauchy stress, restated here for convenience.

$$\boldsymbol{\sigma} = \mathbb{C} : (\boldsymbol{\varepsilon} - \boldsymbol{\varepsilon}^p) \quad (3.20)$$

Next, a constitutive relation is assumed for the micro-stress,

$$\mathbf{T}^p = Y(d^p)\dot{\mathbf{H}}^p, \quad (3.21)$$

where  $d^p$  is an effective distortion rate.

$$d^p = \|\dot{\mathbf{H}}^p\| = \sqrt{\dot{\mathbf{H}}^p : \dot{\mathbf{H}}^p} \quad (3.22)$$

With 3.18, 3.19, and 3.21 in hand, we can revisit the microforce balance, 3.15, and state the flow rule.

$$\mathbf{s} - \left( \operatorname{dev} \operatorname{curl} (k \operatorname{curl} \mathbf{H}^p)^T \right)^T = Y(d^p)\dot{\mathbf{H}}^p \quad (3.23)$$

Attention is drawn to the form of 3.23, which is that of a flow rule with kinematic hardening for  $k > 0$ . In this interpretation,  $\operatorname{dev} \operatorname{curl} (k \operatorname{curl} \mathbf{H}^p)^T$  plays the role of a deviatoric back stress. Rate independent behavior is obtained when the function  $Y(d^p)$  is specified to be  $\sigma_y/d^p$ , where  $\sigma_y$  is the uniaxial yield strength, and this is the form that will be used henceforth.

For the partial differential equation describing the microforce balance, additional boundary conditionals are necessary. For simplicity, we will concentrate on boundary conditions that provide no expenditure of power on the boundary. To begin, we start with the micro-traction condition, 3.16. Then we introduce a projection operator,  $\mathbb{P}(\mathbf{e}) = \mathbf{1} - \mathbf{e} \otimes \mathbf{e}$ , which provides the projection onto the plane perpendicular to  $\mathbf{e}$ . Note that for the skew matrix associated with  $\mathbf{n}$ ,  $(\mathbf{n} \times) \mathbb{P}(\mathbf{n}) = (\mathbf{n} \times)$ , which is true because  $(\mathbf{n} \times)(\mathbf{n} \otimes \mathbf{n}) = (\mathbf{n} \times \mathbf{n}) \otimes \mathbf{n}$  and  $\mathbf{n} \times \mathbf{n} = \mathbf{0}$ . Using the projection, we have

$$\operatorname{dev} (\mathbb{S}^T(\mathbf{n} \times)) : \dot{\mathbf{H}}^p = (\mathbb{S}^T(\mathbf{n} \times)) : \dot{\mathbf{H}}^p \quad (3.24)$$

$$= (\mathbb{S}^T(\mathbf{n} \times) \mathbb{P}(\mathbf{n})) : \dot{\mathbf{H}}^p \quad (3.25)$$

$$= (\mathbb{S}^T(\mathbf{n} \times)) : \dot{\mathbf{H}}^p \mathbb{P}(\mathbf{n}). \quad (3.26)$$

Thus we can arrive at two separate conditions providing a null expenditure of external power, either

$$\operatorname{dev}(\mathbb{S}^T(\mathbf{n}\times)) = 0, \quad (3.27)$$

or

$$\dot{\mathbf{H}}^p(\mathbf{n}\times) = 0, \quad (3.28)$$

where we have utilized the fact that for a tensor  $\mathbf{A}$ ,  $\mathbf{A}\mathbb{P}(\mathbf{n}) = \mathbf{0} \iff \mathbf{A}(\mathbf{n}\times) = \mathbf{0}$ .

Consider the latter, the homogeneous essential boundary condition denoted the *microhard* boundary condition. The microhard condition corresponds to a vanishing flux of the Burgers vector,  $\mathbf{G}^T\mathbf{e}$ , for all planes with normal  $\mathbf{e}$  intersecting  $\Gamma_H$ , where  $\Gamma_H$  is regarded as the microhard boundary. The complementary natural boundary condition corresponds to a micro-stress free boundary,  $\Gamma_S$ , and is referred to as the *microfree* boundary condition.

# Chapter 4

## Variational Formulation

From the previous section we arrived at two partial differential equations, the first describing the macroscopic equilibrium condition, or balance of linear momentum, and the second governing the flow rule for the gradient plasticity model.

$$\operatorname{div} \boldsymbol{\sigma} + \mathbf{b} = \mathbf{0} \quad (4.1)$$

$$\underbrace{\mathbf{T}^p - \mathbf{s}}_{\text{standard term}} + \underbrace{\left( \operatorname{dev} \operatorname{curl} (k \operatorname{curl} \mathbf{H}^p)^{\mathsf{T}} \right)^{\mathsf{T}}}_{\text{gradient term}} = \mathbf{0} \quad (4.2)$$

We will derive a formulation from 4.1 and 4.2, first by noting explicitly how the two equations are coupled. To accomplish this they will be restated solely in terms of  $\mathbf{u}$  and  $\mathbf{H}^p$ .<sup>1</sup>

$$\operatorname{div} \mathbb{C} : (\nabla^s \mathbf{u} - \boldsymbol{\varepsilon}^p) + \mathbf{b} = \mathbf{0} \quad (4.3)$$

$$\frac{Y}{d^p} \dot{\mathbf{H}}^p - \mathbb{C} : (\operatorname{dev} \nabla^s \mathbf{u} - \boldsymbol{\varepsilon}^p) + \left( \operatorname{dev} \operatorname{curl} (k \operatorname{curl} \mathbf{H}^p)^{\mathsf{T}} \right)^{\mathsf{T}} = \mathbf{0} \quad (4.4)$$

It follows that the coupling of the equations comes from the Cauchy stress terms in both equations, specifically the displacement gradient and the symmetric part of  $\mathbf{H}^p$ .

For the equilibrium equation, we proceed to arrive at a weak statement of 4.1, namely integration by parts after multiplying through by a weighting function,  $\mathbf{w}$ , and integrating over the domain. In abstract notation,

$$(\nabla \mathbf{w}, \mathbb{C} : (\nabla^s \mathbf{u} - \boldsymbol{\varepsilon}^p))_{\Omega} = (\mathbf{w}, \mathbf{b})_{\Omega} + (\mathbf{w}, \mathbf{t}(\mathbf{n}))_{\Gamma_t}. \quad (4.5)$$

Where  $\Gamma_t$  is the part of the boundary with prescribed tractions. In a similar fashion, we arrive at a weak statement of 4.2, where now we are using integration by parts to transport a curl over to the weighting function,  $\mathbf{V}$ . First we note that  $\mathbf{A} : \mathbf{B}^{\mathsf{T}} = \mathbf{A}^{\mathsf{T}} : \mathbf{B}$ , and then we use the result of 3.12 on the gradient term of the flow rule and the fact that  $\mathbf{V}$  is constructed to be deviatoric.

$$\left( \mathbf{V}^{\mathsf{T}}, \operatorname{curl} (k \operatorname{curl} \mathbf{H}^p)^{\mathsf{T}} \right)_{\Omega} = (\operatorname{curl} \mathbf{V}, k \operatorname{curl} \mathbf{H}^p)_{\Omega} - (\mathbf{V}, \mathbb{S}^{\mathsf{T}}(\mathbf{n} \times))_{\Gamma} \quad (4.6)$$

Then noting the microtraction condition, 3.16, applicable for the microtraction boundary,  $\Gamma_S$ , the statement of the classical Galerkin weak form of the problem is the following: Find

---

<sup>1</sup>Recall that  $\boldsymbol{\varepsilon}^p = \operatorname{sym} \mathbf{H}^p$ .

$$\{\mathbf{u}, \mathbf{H}^p\} \in \mathcal{S} \times \mathcal{P} \subset H^1(\Omega) \times \text{dev } H^1(\Omega) \text{ s.t. } \forall \{\mathbf{w}, \mathbf{V}\} \in \mathcal{V} \times \mathcal{Q} \subset H^1(\Omega) \times \text{dev } H^1(\Omega)$$

$$(\nabla \mathbf{w}, \boldsymbol{\sigma})_\Omega = (\mathbf{w}, \mathbf{b})_\Omega + (\mathbf{w}, \mathbf{t}(\mathbf{n}))_{\Gamma_t} \quad (4.7)$$

$$(\mathbf{V}, \mathbf{T}^p - \mathbf{s})_\Omega + (\text{curl } \mathbf{V}, k \text{ curl } \mathbf{H}^p)_\Omega = (\mathbf{V}, \mathbf{S}(\mathbf{n}))_{\Gamma_S} \quad (4.8)$$

With two primal fields, the displacements,  $\mathbf{u}$ , and the plastic distortion,  $\mathbf{H}^p$ , the resulting formulation necessarily involves a mixed method. The solution of the displacement field will come in the standard way, using a piecewise continuous basis. The treatment of the flow rule is the main topic for the rest of this section. The classical statement of the gradient plasticity model could be implemented using continuous interpolations for both  $\mathbf{u}$  and  $\mathbf{H}^p$ . However, the solution spaces,  $\mathcal{P}, \mathcal{Q} \subset \text{dev } H^1(\Omega)$  imply a minimum of 32 degrees of freedom for  $\mathbf{H}^{ph} \in \mathcal{P}^1(\Omega_e)$ . If the regularity assumptions can be relaxed, i.e. if we can choose  $\mathcal{P}, \mathcal{Q} \subset \text{dev } L^2(\Omega)$ , then the minimum number of degrees of freedom can be reduced to 8, and, furthermore, larger functional spaces become available. Continuity would still be required, but could be enforced in a weak sense, which motivates use of DG methodology in constructing an alternate variational formulation.

Utilizing the discussion of symmetric interior penalty discontinuous Galerkin methods in Arnold et al. (2002) for motivation, we consider discontinuous  $\mathbf{H}^p$ . After manipulation we arrive at the following equation in terms of interior domains,  $\tilde{\Omega}$  and interior facets,  $\tilde{\Gamma}$ .

$$\begin{aligned} (\mathbf{V}, \mathbf{T}^p - \mathbf{s})_\Omega + (\text{curl } \mathbf{V}, k \text{ curl } \mathbf{H}^p)_{\tilde{\Omega}} \\ + (\llbracket \mathbf{V}, \mathbb{S}^T(\mathbf{n} \times)^T \rrbracket)_{\tilde{\Gamma}} = (\mathbf{V}, \mathbf{S}(\mathbf{n}))_{\Gamma_S} \end{aligned} \quad (4.9)$$

We then apply the following identity to 4.9.

$$\llbracket \mathbf{A}(\mathbf{n} \times) : \mathbf{B} \rrbracket = \llbracket \mathbf{A}(\mathbf{n} \times) \rrbracket : \langle \mathbf{B} \rangle + \langle \mathbf{A} \rangle : \llbracket \mathbf{B}(\mathbf{n} \times)^T \rrbracket \quad (4.10)$$

Now employing 4.10 on the relevant term in 4.9 yields the following.

$$\begin{aligned} (\mathbf{V}, \mathbf{T}^p - \mathbf{s})_\Omega + (\text{curl } \mathbf{V}, k \text{ curl } \mathbf{H}^p)_{\tilde{\Omega}} \\ + (\llbracket \mathbf{V}(\mathbf{n} \times) \rrbracket, \langle \mathbb{S}^T \rangle)_{\tilde{\Gamma}} + (\langle \mathbf{V} \rangle, \llbracket \mathbb{S}^T(\mathbf{n} \times)^T \rrbracket)_{\tilde{\Gamma}} = (\mathbf{V}, \mathbf{S}(\mathbf{n}))_{\Gamma_S} \end{aligned} \quad (4.11)$$

An IP method requires two more pieces, a consistent term for the weak continuity of  $\mathbf{H}^p(\mathbf{n} \times)$ , and a penalty term. The first such term is motivated again by the desire for symmetry with the term that arises naturally through integration by parts.

$$(\langle (k \text{ curl } \mathbf{V})^T \rangle, \llbracket \mathbf{H}^p(\mathbf{n} \times) \rrbracket)_{\tilde{\Gamma}} \quad (4.12)$$

Recall that  $\mathbb{S} = k \text{ curl } \mathbf{H}^p$  from 3.19. The penalty term appears as

$$\frac{\alpha k}{h} (\llbracket \mathbf{V}(\mathbf{n} \times) \rrbracket, \llbracket \mathbf{H}^p(\mathbf{n} \times) \rrbracket)_{\tilde{\Gamma}}. \quad (4.13)$$

Note that the penalty parameter,  $\alpha$ , gets multiplied by the gradient modulus,  $k$ , in 4.13. Lastly, the term with  $\llbracket \mathbb{S}^T(\mathbf{n} \times)^T \rrbracket$  is omitted, as it will return below when the Euler-Lagrange equations are derived to serve the purpose of enforcing continuity of the microtraction.

All the components are in place to state the symmetric DG IP variational formulation for the model of gradient plasticity discussed above. Find  $\{\mathbf{u}^h, \mathbf{H}^{ph}\} \in \mathcal{S}^h \times \mathcal{P}^h \subset H^1(\Omega) \times \text{dev } L^2(\Omega)$  s.t.  $\forall \{\mathbf{w}^h, \mathbf{V}^h\} \in \mathcal{V}^h \times \mathcal{Q}^h \subset H^1(\Omega) \times \text{dev } L^2(\Omega)$  macroscopic equilibrium is satisfied,

$$(\nabla \mathbf{w}^h, \boldsymbol{\sigma}^h)_\Omega = (\mathbf{w}^h, \mathbf{b})_\Omega + (\mathbf{w}^h, \mathbf{t})_{\Gamma_t}, \quad (4.14)$$

and the flow rule is also satisfied,

$$\begin{aligned} & (\mathbf{V}^h, \mathbf{T}^{ph} - \boldsymbol{\sigma}^h)_\Omega + (\text{curl } \mathbf{V}^h, k \text{ curl } \mathbf{H}^{ph})_{\tilde{\Omega}} \\ & + (\llbracket \mathbf{V}^h(\mathbf{n} \times) \rrbracket, \langle \langle (k \text{ curl } \mathbf{H}^{ph})^T \rangle \rangle_{\tilde{\Gamma}})_{\tilde{\Gamma}} + (\langle \langle (k \text{ curl } \mathbf{V}^h)^T \rangle \rangle, \llbracket \mathbf{H}^{ph}(\mathbf{n} \times) \rrbracket)_{\tilde{\Gamma}} \\ & + \frac{\alpha k}{h} (\llbracket \mathbf{V}^h(\mathbf{n} \times) \rrbracket, \llbracket \mathbf{H}^{ph}(\mathbf{n} \times) \rrbracket)_{\tilde{\Gamma}} = (\mathbf{V}^h, \mathbf{S}(\mathbf{n}))_{\Gamma_S}. \end{aligned} \quad (4.15)$$

Variational consistency of the formulation is demonstrated by applying integration by parts to arrive at 4.20–4.24. Note that to recover the curl-curl domain term in the flow rule we need to reverse the steps of the derivation using 4.10 after adding and subtracting the term with  $\llbracket \mathbb{S}^{hT}(\mathbf{n} \times)^T \rrbracket$ . Modelling the steps from the linear elastic case and focusing on the flow rule, we add the following to the method:

$$+(\langle \mathbf{V}^h \rangle, \llbracket \mathbb{S}^{hT}(\mathbf{n} \times)^T \rrbracket)_{\tilde{\Gamma}} - (\langle \mathbf{V}^h \rangle, \llbracket \mathbb{S}^{hT}(\mathbf{n} \times)^T \rrbracket)_{\tilde{\Gamma}}, \quad (4.16)$$

and now we can use 4.10, giving,

$$(\llbracket \mathbf{V}^h, \mathbb{S}^{hT}(\mathbf{n} \times)^T \rrbracket)_{\tilde{\Gamma}} = +(\langle \mathbf{V}^h \rangle, \llbracket \mathbb{S}^{hT}(\mathbf{n} \times)^T \rrbracket)_{\tilde{\Gamma}} + (\llbracket \mathbf{V}^h(\mathbf{n} \times) \rrbracket, \langle \mathbb{S}^{hT} \rangle)_{\tilde{\Gamma}}. \quad (4.17)$$

After these manipulations, the terms remaining in the flow rule can be seen below.

$$\begin{aligned} & (\mathbf{V}^h, \mathbf{T}^{ph} - \boldsymbol{\sigma}^h)_\Omega + (\text{curl } \mathbf{V}^h, k \text{ curl } \mathbf{H}^{ph})_{\tilde{\Omega}} \\ & + (\llbracket \mathbf{V}^h, \mathbb{S}^{hT}(\mathbf{n} \times)^T \rrbracket)_{\tilde{\Gamma}} + (\langle \langle (k \text{ curl } \mathbf{V}^h)^T \rangle \rangle, \llbracket \mathbf{H}^{ph}(\mathbf{n} \times) \rrbracket)_{\tilde{\Gamma}} \\ & - (\langle \mathbf{V}^h \rangle, \llbracket (k \text{ curl } \mathbf{H}^{ph})^T(\mathbf{n} \times) \rrbracket)_{\tilde{\Gamma}} + \frac{\alpha k}{h} (\llbracket \mathbf{V}^h(\mathbf{n} \times) \rrbracket, \llbracket \mathbf{H}^{ph}(\mathbf{n} \times) \rrbracket)_{\tilde{\Gamma}} = (\mathbf{V}^h, \mathbf{S}(\mathbf{n}))_{\Gamma_S}. \end{aligned} \quad (4.18)$$

Integration by parts can be used on 4.18<sub>2,3</sub> to recover the curl-curl domain term.

$$(\mathbf{V}^{hT}, \text{curl}(k \text{ curl } \mathbf{H}^{ph})^T)_\Omega = (\text{curl } \mathbf{V}^h, k \text{ curl } \mathbf{H}^{ph})_{\tilde{\Omega}} + (\llbracket \mathbf{V}^h, \mathbb{S}^{hT}(\mathbf{n} \times)^T \rrbracket)_{\tilde{\Gamma}} \quad (4.19)$$

Similar integration by parts occurs for the macroscopic equilibrium equation in the standard way. The resulting Euler-Lagrange equations are stated below.

$$(\mathbf{w}^h, \text{div } \boldsymbol{\sigma}^h + \mathbf{b})_\Omega = 0 \quad (4.20)$$

$$(\mathbf{V}^h, \mathbf{T}^{ph} - \boldsymbol{\sigma}^h + (\text{curl}(k \text{ curl } \mathbf{H}^{ph})^T)^T)_{\tilde{\Omega}} = 0 \quad (4.21)$$

$$\langle \langle (k \text{ curl } \mathbf{V}^h)^T \rangle \rangle, \llbracket \mathbf{H}^{ph}(\mathbf{n} \times) \rrbracket)_{\tilde{\Gamma}} = 0 \quad (4.22)$$

$$\langle \mathbf{V}^h \rangle, \llbracket (k \text{ curl } \mathbf{H}^{ph})^T(\mathbf{n} \times) \rrbracket)_{\tilde{\Gamma}} = 0 \quad (4.23)$$

$$(\mathbf{V}^h, (\mathbb{S}^T(\mathbf{n} \times) - \mathbf{S}(\mathbf{n})))_{\Gamma_S} = 0 \quad (4.24)$$

From these Euler-Lagrange equations it is clear that the exact solution also satisfies the interior penalty discontinuous Galerkin weak form 4.14 and 4.15, which is the classical requirement for consistency of a finite element formulation. Note that 4.23 is equivalently expressed as  $\left(\langle \mathbf{V}^h \rangle, \llbracket \mathbb{S}^{h^T}(\mathbf{n} \times) \rrbracket\right)_{\bar{\Gamma}} = 0$ , implying continuity of the microtraction in a weak sense. Now note that, using standard arguments about the arbitrariness of the weighting function,  $\mathbf{V}$ , we have enforced the flow rule, and weak continuity of the primal field and the microtraction, verifying consistency.

# Chapter 5

## Implementation

Implementation of the model is carried out in a nonlinear finite element code using a Newton-Raphson iterative procedure. The displacement field is chosen to be  $\mathcal{C}^0$  continuous, or piecewise continuous, in the standard way, while the plastic displacement gradient field is chosen to be  $\mathcal{C}^{-1}$  continuous, and either piecewise constant or linear and discontinuous across subdomains.

### 5.1 Mixed Plasticity

Consider the formulation presented above without the gradient terms, which is the analog for classical plasticity in a two-field setting. The variational statement reads as follows: find  $\{\delta \mathbf{u}^h, \delta \mathbf{H}^{ph}\} \in \mathcal{S}^h \times \mathcal{P}^h \subset H^1(\Omega) \times \text{dev } L^2(\Omega)$  s.t.  $\forall \{\mathbf{w}^h, \mathbf{V}^h\} \in \mathcal{V}^h \times \mathcal{Q}^h \subset H^1(\Omega) \times \text{dev } L^2(\Omega)$  macroscopic equilibrium is satisfied,

$$(\nabla \mathbf{w}^h, \boldsymbol{\sigma}^h)_\Omega = 0, \quad (5.1)$$

and the flow rule is also satisfied,

$$(\mathbf{V}^h, \mathbf{T}^{ph} - \boldsymbol{\sigma}^h)_\Omega = 0. \quad (5.2)$$

The interpolations for the solution and variational fields are defined as

$$\delta \mathbf{u}^h = \sum_a^{n_{nodes}} \mathbf{N}^a \mathbf{d}^a \quad \delta \mathbf{w}^h = \sum_a^{n_{nodes}} \mathbf{N}^a \mathbf{c}^a, \quad (5.3)$$

$$\delta \mathbf{H}^{ph} = \sum_b^{n_p} \boldsymbol{\phi}^b \boldsymbol{\eta}^b \quad \delta \mathbf{V}^h = \sum_b^{n_p} \boldsymbol{\phi}^b \boldsymbol{\theta}^b, \quad (5.4)$$

where the index  $a$  cycles through the number of nodes in the element, and the index  $b$  cycles through the number of integration points used to represent the  $\mathbf{H}^p$  degrees of freedom. Henceforth, for notational simplicity, the superscript  $h$  denoting finite dimensional approximations, will be dropped. The resulting system differs from the classical plasticity model in the sense that the flow rule will now be satisfied globally, where in the classical setting consistency is satisfied locally at each integration point.

As in the standard case, a yield surface needs to be defined. Recall the classical construction of a yield surface including a backstress, call it  $\boldsymbol{\beta}$ . We formulate the yield surface as follows.

$$f(\boldsymbol{\sigma}, \boldsymbol{\beta}) := \|\boldsymbol{s} - \boldsymbol{\beta}\| - \sqrt{\frac{2}{3}}\sigma_y \quad (5.5)$$

And the restriction holds that  $f \leq 0$ .

The temporal solution is achieved via a backward Euler time integration scheme, therefore the solution procedure is implicit. To do this, a given time step is concerned with advancing the solution from the time  $t_n$  to the time  $t_{n+1}$ , where the time step  $\Delta t$  is then defined as  $t_{n+1} - t_n$ . Since the data at  $t_n$  is known (as it is potentially a converged solution), the algorithm is constructed using plastic quantities defined at  $t_n$ . To begin, we will define some algorithmic quantities below. Consider the Cauchy stress at time  $t_{n+1}$ .

$$\boldsymbol{\sigma}_{n+1} = \mathbb{C} : (\boldsymbol{\varepsilon}_{n+1} - \boldsymbol{\varepsilon}_{n+1}^p) \quad (5.6)$$

Where  $\boldsymbol{\varepsilon}_{n+1} = \nabla^s \mathbf{u}_{n+1}$  and  $\boldsymbol{\varepsilon}_{n+1}^p = \text{sym } \mathbf{H}_{n+1}^p$ . For the microstress  $\mathbf{T}^p$  we need to approximate the quantity  $\dot{\mathbf{H}}^p$ .

$$\mathbf{T}_{n+1}^p = \frac{\sigma_y}{d^p} \dot{\mathbf{H}}^p \approx \frac{\sigma_y}{d^p} \left( \frac{\mathbf{H}_{n+1}^p - \mathbf{H}_n^p}{\Delta t} \right) \quad (5.7)$$

Recall the equation for  $d^p$ , 3.22 which can be approximated as

$$d_{n+1}^p \approx \left\| \frac{\mathbf{H}_{n+1}^p - \mathbf{H}_n^p}{\Delta t} \right\| = \frac{\|\mathbf{H}_{n+1}^p - \mathbf{H}_n^p\|}{\Delta t}. \quad (5.8)$$

Combining 5.7 and 5.8 the time step factors cancel by construction, which necessitates rate independent stress. A simplified representation of the microstress, without the time step factors, can be seen in 5.9, which has the form of a magnitude times a direction. Note that for this formulation, the magnitude of  $\mathbf{T}^p$  is fixed to be  $\sigma_y$ .

$$\mathbf{T}_{n+1}^p = \sigma_y \left( \frac{\mathbf{H}_{n+1}^p - \mathbf{H}_n^p}{\|\mathbf{H}_{n+1}^p - \mathbf{H}_n^p\|} \right) \quad (5.9)$$

A predictor-corrector solution strategy is used. A discussion of the strategy follows below, and the algorithm can be seen in Algorithm 5.1. A trial state is evaluated and the yield condition is checked during the predictor stage, and solution of the flow rule is computed for the set of elements that have violated the yield condition in the corrector stage. This solution strategy is analogous to that of classical plasticity, the main difference being the global solution of the flow rule PDE in the gradient plasticity case, versus the local solution in the classical case.

For the predictor stage, we first apply the Dirichlet boundary conditions assuming elastic constitutive behavior and solve to get an initial guess for the displacement field at  $t_{n+1}$ .

---

**Algorithm 5.1** Predictor-corrector algorithm for gradient plasticity, global equilibrium iteration  $j$ , and time step  $n + 1$

---

**Predictor stage**

**if**  $j == 0$  **then**

    Use elastic tangent

**else**

    Compute trial state

**for** each element **do**

$$\boldsymbol{\sigma}_{n+1,j}^{\text{tr}} = \mathbb{C} : (\nabla^s \mathbf{u}_{n+1} - \boldsymbol{\varepsilon}_n^p)$$

$$\boldsymbol{\beta}_{n+1,j}^{\text{tr}} = \boldsymbol{\beta}_n$$

$$f^{\text{tr}} = f(\boldsymbol{\sigma}_{n+1,j}^{\text{tr}}, \boldsymbol{\beta}_{n+1,j}^{\text{tr}})$$

**if**  $f \geq 0$  **then**

        Add current element to list of plastic elements

**else**

$$\boldsymbol{\sigma}_{n+1,j} = \boldsymbol{\sigma}_{n+1,j}^{\text{tr}}$$

**end if**

**end for**

**end if**

**Corrector stage**

**while** flow rule residual,  $\|\mathbf{R}_{n+1,k}^p\| > \text{TOL}$  **do**

**for** each element in set of plastic elements **do**

        Compute plastic quantities

$$\Delta \mathbf{H}_{n+1,k}^p = \mathbf{H}_{n+1,k}^p - \mathbf{H}_n^p$$

$$\tilde{d}_{n+1,k}^p = \|\Delta \mathbf{H}_{n+1,k}^p\|$$

$$\mathbf{T}_{n+1,k}^p = \frac{\sigma_y}{\tilde{d}_{n+1,k}^p} \Delta \mathbf{H}_{n+1,k}^p$$

$$\boldsymbol{\sigma}_{n+1} = \mathbb{C} : (\nabla^s \mathbf{u}_{n+1} - \boldsymbol{\varepsilon}_{n+1,k}^p)$$

**end for**

    Assemble  $\mathbf{K}_{n+1,k}^p$ ,  $\mathbf{R}_{n+1,k}^p$

    Solve 5.21 and update  $\mathbf{H}_{n+1,k+1}^p = \mathbf{H}_{n+1,k}^p + \delta \mathbf{H}^p$

    Increment flow rule iteration,  $k \rightarrow k + 1$

**end while**

Assemble global equilibrium 5.34 solve for  $\mathbf{u}_{n+1,j+1}$

Check for global convergence

**if**  $\|\mathbf{R}_{n+1,j}^{eq}\| < \text{TOL}$  **then**

    Advance state  $(\cdot)_{n+1} \rightarrow (\cdot)_n$

**else**

    Increment equilibrium iteration,  $j \rightarrow j + 1$ , return to predictor

**end if**

---

Then we define the trial state with respect to the displacements at time  $t_{n+1}$ , but the plastic fields at time  $t_n$ , as mentioned above. Again,  $(\cdot)^{\text{tr}}$  denotes a quantity in its trial state.

$$\boldsymbol{\sigma}_{n+1}^{\text{tr}} = \mathbb{C} : (\nabla^s \mathbf{u}_{n+1} - \boldsymbol{\varepsilon}_n^p) \quad (5.10)$$

$$\boldsymbol{\beta}_{n+1}^{\text{tr}} = \boldsymbol{\beta}_n \quad (5.11)$$

$$f_{n+1}^{\text{tr}} = f(\boldsymbol{\sigma}_{n+1}^{\text{tr}}, \boldsymbol{\beta}_{n+1}^{\text{tr}}) \quad (5.12)$$

Now the yield condition is evaluated using 5.5, and any element that violates the requirement that  $f \leq 0$  is determined to be in the set of plastic elements.

In the corrector stage, the flow rule PDE is assembled and solved in an iterative fashion using a Newton-Raphson method. We assume that the displacement field, and thus the strain, is constant during the iterative solve of the flow rule. In this sense the method proposed is a staggered approach at solving a coupled pair of PDEs. In order to assemble the system, certain quantities need to be computed. The first of these is the incremental quantity  $\Delta \mathbf{H}_{n+1,k}^p$ , where  $k$  is the current iterate in the flow rule iterative solve.

$$\Delta \mathbf{H}_{n+1,k}^p = \mathbf{H}_{n+1,k}^p - \mathbf{H}_n^p \quad (5.13)$$

Then a rate independent approximation for  $d^p$  is made as

$$\tilde{d}_{n+1,k}^p = \|\Delta \mathbf{H}_{n+1,k}^p\|, \quad (5.14)$$

from which  $\mathbf{T}_{n+1,k}^p$  is computed as

$$\mathbf{T}_{n+1,k}^p = \frac{\sigma_y}{\tilde{d}_{n+1,k}^p} \Delta \mathbf{H}_{n+1,k}^p. \quad (5.15)$$

To evaluate the Cauchy stress, the plastic strain is computed and the stress is calculated via 5.6. Equations 5.15 and 5.6 define the microstress and the Cauchy stress, which are regarded as element quantities in the set of plastic elements that make up the plastic domain. The other term from 5.36 considers quantities defined on the interior facets of the plastic domain, and uses the current iterate of  $\mathbf{H}_{n+1,k}^p$  and the normal vector for the facet being integrated, meaning that no fields need to be computed to assemble that term. The residual for the method then comes from assembling the variational form with the current iterate.

$$\mathcal{R}_{n+1,k}^p = (\mathbf{V}, \mathbf{T}_{n+1,k}^p - \boldsymbol{\sigma}_{n+1})_{\Omega} \quad (5.16)$$

When assembled into matrix form, 5.16 can be expressed as

$$\boldsymbol{\theta}^T \{ \mathbf{R}_{n+1,k}^p \}, \quad (5.17)$$

where the vector  $\boldsymbol{\theta}$  are the degrees of freedom associated with  $\mathbf{V}$ , as seen in 5.4. Lastly, the flow rule needs to be linearized with respect to an increment in  $\mathbf{H}^p$ . The approach taken is a first-order Taylor expansion of the residual.

$$\mathcal{R}_{n+1,k+1} = \mathcal{R}_{n+1,k} + \frac{\partial \mathcal{R}_{n+1,k}}{\partial \mathbf{H}^p} : \delta \mathbf{H}^p = 0 \quad (5.18)$$

The linearization of the flow rule is shown below for the case of perfect plasticity.

$$\frac{\partial \mathcal{R}_{n+1,k}}{\partial \mathbf{H}^p} : \delta \mathbf{H}^p = \left( \mathbf{V}, \left[ \frac{\sigma_y}{\tilde{d}_{n+1,k}^p} \mathbf{1} \otimes \mathbf{1} - \frac{\sigma_y}{\tilde{d}_{n+1,k}^3} \Delta \mathbf{H}_{n+1,k}^p \otimes \Delta \mathbf{H}_{n+1,k}^p + \mathbb{C} \right] : \delta \mathbf{H}^p \right)_{\Omega} \quad (5.19)$$

From 5.19, the consistent tangent can be assembled into the stiffness matrix for the flow rule,  $\mathbf{K}_{n+1,k}^p$ , and iteratively solved for  $\delta \mathbf{H}_k^p$ , the increment in the plastic distortion. In matrix form the system for the flow rule, 5.18, looks as

$$\boldsymbol{\theta}^T \{ \mathbf{R}_{n+1,k}^p \} + \boldsymbol{\theta}^T [ \mathbf{K}_{n+1,k}^p ] \boldsymbol{\eta} = 0, \quad (5.20)$$

where  $\boldsymbol{\eta}$  is the vector of degrees of freedom associated with  $\delta \mathbf{H}^p$ . Due to the arbitrariness of the variational degrees of freedom  $\boldsymbol{\theta}$ , we arrive at the following system, for  $\boldsymbol{\eta}$ .

$$[ \mathbf{K}_{n+1,k}^p ] \boldsymbol{\eta} = - \mathbf{R}_{n+1,k}^p \quad (5.21)$$

Then the iteration proceeds with the update of the field using 5.21 and the interpolations for  $\delta \mathbf{H}^p$  in 5.4

$$\mathbf{H}_{n+1,k+1}^p = \mathbf{H}_{n+1,k}^p + \delta \mathbf{H}_k^p, \quad (5.22)$$

and  $k \rightarrow k + 1$ .

The solution of the equilibrium equation follows a successful solution of the flow rule. In a similar fashion the  $\mathbf{H}^p$  degrees of freedom are held constant during this solve, and further, the fact that the flow rule has been satisfied is exploited, which essentially allows the whole mixed system to be assembled and solved. The global equilibrium residual, absent body forces, for iterate  $j$ , is constructed as

$$\mathcal{R}_{n+1,j}^{eq} = (\nabla \mathbf{w}, \boldsymbol{\sigma}_{n+1,j})_{\Omega} \quad (5.23)$$

which in matrix form appears as,

$$\mathbf{c}^T \{ \mathbf{R}_{n+1,j}^{eq} \}. \quad (5.24)$$

Now we can consider the complete, mixed system consisting of the equilibrium equation and the flow rule. After relatively simple linearization, the mixed tangent can be split into partitions defined as

$$(\nabla \mathbf{w}, \mathbb{C} : \nabla^s \delta \mathbf{u}) \quad (5.25)$$

$$+ (\nabla \mathbf{w}, -\mathbb{C} : (\text{sym } \delta \mathbf{H}^p))_{\Omega} \quad (5.26)$$

$$+ (\mathbf{V}, -\mathbb{C} : \nabla^s \delta \mathbf{u})_{\Omega} \quad (5.27)$$

$$+ \left( \mathbf{V}, \left[ \frac{\sigma_y}{\tilde{d}_{n+1,k}^p} \mathbf{1} \otimes \mathbf{1} - \frac{\sigma_y}{\tilde{d}_{n+1,k}^3} \Delta \mathbf{H}_{n+1,k}^p \otimes \Delta \mathbf{H}_{n+1,k}^p + \mathbb{C} \right] : \delta \mathbf{H}^p \right)_{\Omega} \quad (5.28)$$

which lead to the matrix equations for the linearized global equilibrium system.

$$\begin{Bmatrix} \mathbf{c} \\ \boldsymbol{\theta} \end{Bmatrix}^T \left( \begin{Bmatrix} \mathbf{R}_{n+1,j}^{eq} \\ \mathbf{R}_{n+1,j}^p \end{Bmatrix} + \begin{bmatrix} \mathbf{K}_{n+1,j}^{uu} & \mathbf{K}_{n+1,j}^{up} \\ \mathbf{K}_{n+1,j}^{pu} & \mathbf{K}_{n+1,j}^{pp} \end{bmatrix} \begin{Bmatrix} \mathbf{d} \\ \boldsymbol{\eta} \end{Bmatrix} \right) = 0 \quad (5.29)$$

The result of 5.29, when considering the arbitrariness of the variations, is the system of equations seen below.

$$\begin{bmatrix} \mathbf{K}_{n+1,j}^{uu} & \mathbf{K}_{n+1,j}^{up} \\ \mathbf{K}_{n+1,j}^{pu} & \mathbf{K}_{n+1,j}^{pp} \end{bmatrix} \begin{Bmatrix} \mathbf{d} \\ \boldsymbol{\eta} \end{Bmatrix} = - \begin{Bmatrix} \mathbf{R}_{n+1,j}^{eq} \\ \mathbf{R}_{n+1,j}^p \end{Bmatrix} \quad (5.30)$$

Note that the matrix  $\mathbf{K}_{n+1,j}^{pp}$  is precisely the same matrix from the converged solution of the flow rule,  $\mathbf{K}_{n+1,k}^p$ . Consider the global system in 5.30, which can be written into two equations.

$$\mathbf{K}_{n+1,j}^{uu} \mathbf{d} + \mathbf{K}_{n+1,j}^{up} \boldsymbol{\eta} = -\mathbf{R}_{n+1,j}^{eq} \quad (5.31)$$

$$\mathbf{K}_{n+1,j}^{pu} \mathbf{d} + \mathbf{K}_{n+1,j}^{pp} \boldsymbol{\eta} = -\mathbf{R}_{n+1,j}^p \quad (5.32)$$

Concentrating on 5.32, we can exploit that fact that we have solved the flow rule PDE and set  $\mathbf{R}_{n+1,j}^p = \mathbf{0}$ . Then, solve for the vector  $\boldsymbol{\eta}$ , in terms of the displacement degrees of freedom  $\mathbf{d}$ .

$$\boldsymbol{\eta} = - [\mathbf{K}_{n+1,j}^{pp}]^{-1} \mathbf{K}_{n+1,j}^{pu} \mathbf{d} \quad (5.33)$$

Now we can use the result of 5.33 by substitution into 5.31 to arrive at the following equation.

$$\left( \mathbf{K}_{n+1,j}^{uu} - \mathbf{K}_{n+1,j}^{up} [\mathbf{K}_{n+1,j}^{pp}]^{-1} \mathbf{K}_{n+1,j}^{pu} \right) \mathbf{d} = -\mathbf{R}_{n+1,j}^{eq} \quad (5.34)$$

The previous process is not unlike static condensation for a local field, however the matrix to be inverted in this case,  $[\mathbf{K}_{n+1,j}^{pp}]$ , is global by nature due to the interior facet terms, and cannot be reduced down to a matrix inversion at the element level.

## 5.2 Constant Basis for $H^p$

This choice of space for  $H^p$  significantly reduces the number of degrees of freedom necessary for representation, as mentioned above, and also simplifies the notion of boundary conditions for the flow rule PDE. The microhard and microfree boundary conditions apply only to the boundary of the plastic domain, and thus for linear or higher-order fields, it would be possible for the elastic-plastic boundary to exist within elements and special consideration would be necessary to properly define the normal vector and hence apply boundary conditions. For piecewise constant plastic fields, the most natural decision is to use the element faces which are already available, and no additional surfaces need to be created to apply boundary conditions.

Using piecewise constants for  $H^p$  simplifies the variational formulation since all the curl terms evaluate to zero. The benefit of this is simplicity and efficiency, while the drawback is the gradient term being inseparable from the penalty term. Also, we will be considering only Dirichlet boundary conditions and no body forces, which further simplifies the formulation. Lastly, the solution procedure will be solving for increments in displacement and plastic distortion, and so interpolations will be written for incremental quantities. For completeness,

the simplified variational form is stated as: find  $\{\delta \mathbf{u}^h, \delta \mathbf{H}^{ph}\} \in \mathcal{S}^h \times \mathcal{P}^h \subset H^1(\Omega) \times \text{dev } L^2(\Omega)$  s.t.  $\forall \{\mathbf{w}^h, \mathbf{V}^h\} \in \mathcal{V}^h \times \mathcal{Q}^h \subset H^1(\Omega) \times \text{dev } L^2(\Omega)$  macroscopic equilibrium is satisfied,

$$(\nabla \mathbf{w}^h, \boldsymbol{\sigma}^h)_\Omega = 0, \quad (5.35)$$

and the flow rule is also satisfied,

$$(\mathbf{V}^h, \mathbf{T}^{ph} - \boldsymbol{\sigma}^h)_\Omega + \frac{\alpha k}{h} (\llbracket \mathbf{V}^h(\mathbf{n} \times) \rrbracket, \llbracket \mathbf{H}^{ph}(\mathbf{n} \times) \rrbracket)_{\tilde{\Gamma}} = 0. \quad (5.36)$$

Note the additional term in the flow rule formulation as compared to the mixed plasticity case 5.2. Since we will be using piecewise constants to interpolate  $\mathbf{H}^p$ , we will only have one integration point per element. Also the basis functions in 5.4 will simply be identity matrices. The resulting system differs from the classical plasticity model in a number of ways. First, due to the gradient term, the plastic fields are governed by a PDE, with implications of a larger system of equations to solve. Second, the system of equations now includes a term defined on the interior facets,  $\tilde{\Gamma}$ , stemming from the DG formulation. Third, the plastic field  $\mathbf{H}^p$  is not necessarily a symmetric tensor, and in fact, its deviation from symmetry will solely come from the gradient term.

The yield surface, 5.37, needs to be modified to account for DG term. Recall that the gradient term has the appearance of a backstress, call it  $\boldsymbol{\zeta}$ , in the flow rule. Then we formulate the yield surface.

$$f(\boldsymbol{\sigma}, \boldsymbol{\beta}, \boldsymbol{\zeta}) := \|\mathbf{s} - \boldsymbol{\zeta}\| - \sqrt{\frac{2}{3}} \sigma_y \quad (5.37)$$

And, again, the restriction holds that  $f \leq 0$ .

Time integration is performed within the framework of the mixed plasticity algorithm presented above, 5.1. The additional term from 5.36, compared to the mixed plasticity case, considers quantities defined on the interior facets of the plastic domain, and uses the current iterate of  $\mathbf{H}_{n+1,k}^p$  and the normal vector for the facet being integrated, meaning that no fields need to be computed to assemble that term. The residual for the method then comes from assembling the variational form with the current iterate.

$$\mathcal{R}_{n+1,k}^p = (\mathbf{V}, \mathbf{T}_{n+1,k}^p - \boldsymbol{\sigma}_{n+1})_\Omega + \frac{\alpha k}{h} (\llbracket \mathbf{V}(\mathbf{n} \times) \rrbracket, \llbracket \mathbf{H}_{n+1,k}^p(\mathbf{n} \times) \rrbracket)_{\tilde{\Gamma}} \quad (5.38)$$

When assembled into matrix form, 5.38 can be expressed as

$$\boldsymbol{\theta}^T \{ \mathbf{R}_{n+1,k}^p \}, \quad (5.39)$$

where the vector  $\boldsymbol{\theta}$  are the degrees of freedom associated with  $\mathbf{V}$ , as seen in 5.4. Lastly, the flow rule needs to be linearized with respect to an increment in  $\mathbf{H}^p$ . The linearization is

performed as seen above.

$$\begin{aligned} \frac{\partial \mathcal{R}_{n+1,k}}{\partial \mathbf{H}^p} : \delta \mathbf{H}^p = & \\ \left( \mathbf{V}, \left[ \frac{\sigma_y}{\tilde{d}_{n+1,k}^p} \mathbf{1} \otimes \mathbf{1} - \frac{\sigma_y}{\tilde{d}_{n+1,k}^3} \Delta \mathbf{H}_{n+1,k}^p \otimes \Delta \mathbf{H}_{n+1,k}^p + \mathbb{C} \right] : \delta \mathbf{H}^p \right)_{\Omega} & \quad (5.40) \\ + \frac{\alpha k}{h} (\llbracket \mathbf{V}(\mathbf{n} \times) \rrbracket, \llbracket \delta \mathbf{H}^p(\mathbf{n} \times) \rrbracket)_{\bar{\Gamma}} & \end{aligned}$$

Now 5.40 is used to assemble the stiffness matrix for the flow rule,  $\mathbf{K}_{n+1,k}^p$ , and iteratively solved for  $\delta \mathbf{H}_k^p$ .

The gradient backstress,  $\boldsymbol{\zeta}_{n+1}$ , comes directly from the flow rule, 4.2, and as such is defined as

$$\boldsymbol{\zeta}_{n+1} = \left( \text{dev curl} \left( k \text{ curl } \mathbf{H}_{n+1}^p \right)^{\text{T}} \right)^{\text{T}}. \quad (5.41)$$

However, the choice of a constant basis for  $\mathbf{H}^p$  renders 5.41 insufficient to determine the backstress, since the curl terms evaluate to zero. In order to construct a consistent backstress the variational form of the flow rule, and specifically the fact that it is driven to zero, is exploited. Given a converged solution of the flow rule where we are substituting 5.41 in for the gradient term,

$$\mathbf{T}_{n+1}^p - \text{dev } \boldsymbol{\sigma}_{n+1} + \boldsymbol{\zeta}_{n+1} = \mathbf{0}, \quad (5.42)$$

we can approximate the back stress as,

$$\boldsymbol{\zeta}_{n+1} \approx \mathbf{T}_{n+1}^p - \text{dev } \boldsymbol{\sigma}_{n+1}. \quad (5.43)$$

Inspection of the method shows that for a gradient modulus of zero,  $k = 0$ ,  $\mathbf{T}_{n+1}^p = \text{dev } \boldsymbol{\sigma}_{n+1}$  and no backstress is accumulated. Intuitively, the backstress term comes directly from the interior facet gradient term. In practice, once the flow rule solution procedure has converged,  $\boldsymbol{\zeta}_{n+1}$  is calculated, and the solution of macroscopic equilibrium follows.

### 5.3 Linear Basis for $\mathbf{H}^p$

As pointed out in section 5.2, using a constant basis within an element reduces the number of necessary degrees of freedom in the flow rule system. However, as was also noted, the interior penalty term coincides with the remaining term from the flow rule, which is undesirable. For that reason, a piecewise linear basis within an element, but still discontinuous across elements, is also being explored. This choice of basis introduces additional technical difficulties, including the need to define the elastic-plastic domain boundaries in order to apply the gradient boundary conditions, as well as the adding bookkeeping of dealing with jumps and averages of linear fields pertaining to the integrals over the interior facets.

Now the variational statement for the flow rule will include all the terms from (4.15), restated here for completeness.

$$\begin{aligned}
& (\mathbf{V}^h, \mathbf{T}^{ph} - \boldsymbol{\sigma}^h)_\Omega + (\text{curl } \mathbf{V}^h, k \text{ curl } \mathbf{H}^{ph})_{\tilde{\Omega}} \\
& + (\llbracket \mathbf{V}^h(\mathbf{n} \times) \rrbracket, \langle \langle (k \text{ curl } \mathbf{H}^{ph})^T \rangle \rangle_{\tilde{\Gamma}})_{\tilde{\Gamma}} + (\langle \langle (k \text{ curl } \mathbf{V}^h)^T \rangle \rangle, \llbracket \mathbf{H}^{ph}(\mathbf{n} \times) \rrbracket)_{\tilde{\Gamma}} \\
& + \frac{\alpha k}{h} (\llbracket \mathbf{V}^h(\mathbf{n} \times) \rrbracket, \llbracket \mathbf{H}^{ph}(\mathbf{n} \times) \rrbracket)_{\tilde{\Gamma}} = (\mathbf{V}^h, \mathbf{S}(\mathbf{n}))_{\Gamma_S}.
\end{aligned} \tag{5.44}$$

As above, the superscript  $h$  is dropped for notational convenience.

The residual now includes the jump-average and average-jump terms arising from the integration by parts of the curl term.

$$\mathcal{R}_{n+1,k}^p = (\mathbf{V}, \mathbf{T}_{n+1,k}^p - \boldsymbol{\sigma}_{n+1})_\Omega + (\text{curl } \mathbf{V}, k \text{ curl } \mathbf{H}^p)_{\tilde{\Omega}} \tag{5.45}$$

$$+ (\llbracket \mathbf{V}(\mathbf{n} \times) \rrbracket, \langle \langle (k \text{ curl } \mathbf{H}^p)^T \rangle \rangle_{\tilde{\Gamma}})_{\tilde{\Gamma}} + (\langle \langle (k \text{ curl } \mathbf{V})^T \rangle \rangle, \llbracket \mathbf{H}^p(\mathbf{n} \times) \rrbracket)_{\tilde{\Gamma}} \tag{5.46}$$

$$+ \frac{\alpha k}{h} (\llbracket \mathbf{V}(\mathbf{n} \times) \rrbracket, \llbracket \mathbf{H}_{n+1,k}^p(\mathbf{n} \times) \rrbracket)_{\tilde{\Gamma}} \tag{5.47}$$

After linearization, the tangent can be written with the additional terms.

$$\frac{\partial \mathcal{R}_{n+1,k}}{\partial \mathbf{H}^p} : \delta \mathbf{H}^p = \left( \mathbf{V}, \left[ \frac{\sigma_y}{\tilde{d}_{n+1,k}^p} \mathbf{1} \otimes \mathbf{1} - \frac{\sigma_y}{\tilde{d}_{n+1,k}^p{}^3} \Delta \mathbf{H}_{n+1,k}^p \otimes \Delta \mathbf{H}_{n+1,k}^p + \mathbb{C} \right] : \delta \mathbf{H}^p \right)_\Omega \tag{5.48}$$

$$+ (\text{curl } \mathbf{V}, k \text{ curl } \mathbf{H}^p)_{\tilde{\Omega}} \tag{5.49}$$

$$+ (\llbracket \mathbf{V}(\mathbf{n} \times) \rrbracket, \langle \langle (k \text{ curl } \mathbf{H}^p)^T \rangle \rangle_{\tilde{\Gamma}})_{\tilde{\Gamma}} + (\langle \langle (k \text{ curl } \mathbf{V})^T \rangle \rangle, \llbracket \mathbf{H}^p(\mathbf{n} \times) \rrbracket)_{\tilde{\Gamma}} \tag{5.50}$$

$$+ \frac{\alpha k}{h} (\llbracket \mathbf{V}(\mathbf{n} \times) \rrbracket, \llbracket \delta \mathbf{H}^p(\mathbf{n} \times) \rrbracket)_{\tilde{\Gamma}} \tag{5.51}$$

Using the previous terms, (5.45) and (5.48), in the first order Taylor expansion of the residual, (5.18), in the mixed plasticity framework yield yields the algorithm for the choice of linear basis functions. The yield condition via the exploitation of the flow rule now includes the curl-curl terms from the interior domain integrals, as well as the other DG terms. At the time of this writing the elastic-plastic domain is still being considered as coinciding with element boundaries. Essentially, the boundary exists between active and inactive elements, where active elements are considered as those elements who have violated the yield condition as well as neighboring elements who become active due to the presence of the DG terms.



# Chapter 6

## Results

Results for the mixed plasticity algorithm, constant interpolations, and linear interpolations follow. The first implementation was done in FEniCS. Subsequent development using the linear basis have been performed in Matlab.

### 6.1 Mixed Plasticity

Initially, an implementation of the mixed plasticity algorithm was executed using the FEniCS project. At the time, FEniCS did not support the usage of three dimensional elements that were not tetrahedral. To verify the mixed plasticity implementation, we will look at the convergence of a torsional boundary value problem (BVP) with mesh refinement. Torsion produces a gradient in the strain field, and will be used to show proper convergence for both perfect plasticity and isotropic hardening. A schematic of the problem can be seen in Figure 6.1, which shows that one end of the cylinder is fixed in all three degrees of freedom, while the other end of the cylinder is given a prescribed rotation in the  $\theta$  direction.

First consider the case of perfect plasticity, which coincides with a hardening parameter of zero. This means that the deviatoric stress in the body cannot exceed a certain value, no matter how much the body is deformed. This is a useful test since we can obtain, in the asymptotic limit, an analytical solution for the torque when the cylinder has entered the fully plastic regime. From elasticity we know that the torque on a circular cross section is equal to the integral over the area of the shear stress multiplied by the radius. In this case the shear stress is limited by perfect plasticity to be  $\tau_y = \sigma_y/\sqrt{3}$ , where  $\tau_y$  is the yield stress in shear and  $\sigma_y$  in the uni-axial yield strength. An expression for the torque follows.

$$T = \int_A (\tau_y r) r \, dr \, d\theta \quad (6.1)$$

$$T = \frac{\sigma_y 2\pi R^3}{3\sqrt{3}} \quad (6.2)$$

For the particular problem in question, with material constants from Table 6.1, the analytical solution for the applied torque is  $T = 147.371$  [N-mm]. In Figure 6.2 torque versus radians of twist are plotted for increasingly fine mesh densities. Each curve is labeled by a mesh number. The number of tetrahedral elements for each mesh can be found in Table 6.2.

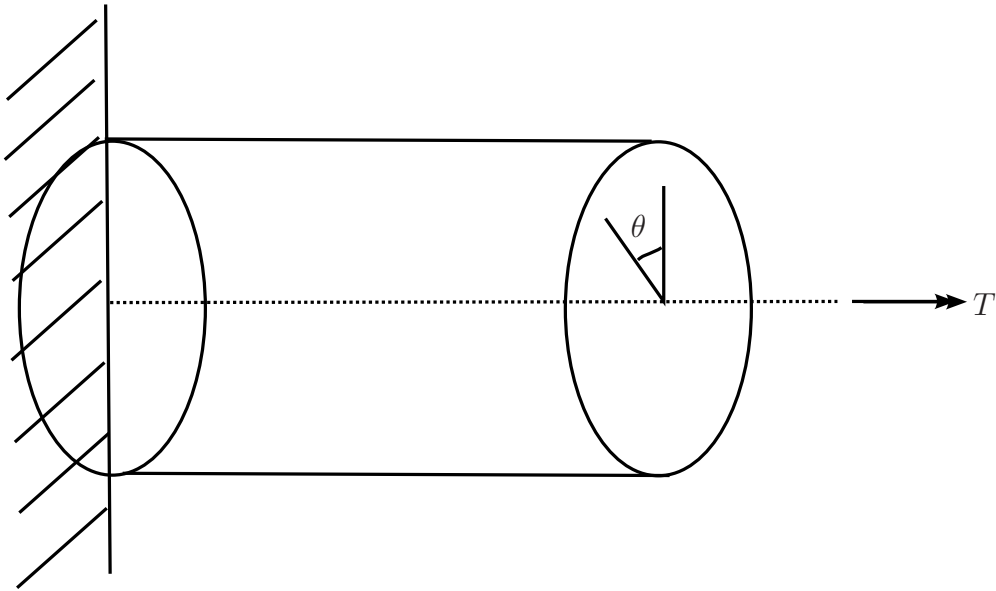


**Figure 6.1.** Schematic of the torsion BVP

Parameter	Value [units]
Young's modulus, $E$	200.0E3 [MPa]
Poisson's ratio, $\nu$	0.3
Yield strength, $\sigma_y$	975.0 [MPa]
Cylinder radius, $R$	0.5 [mm]

**Table 6.1.** Parameters used in the simulation of the torsion BVP

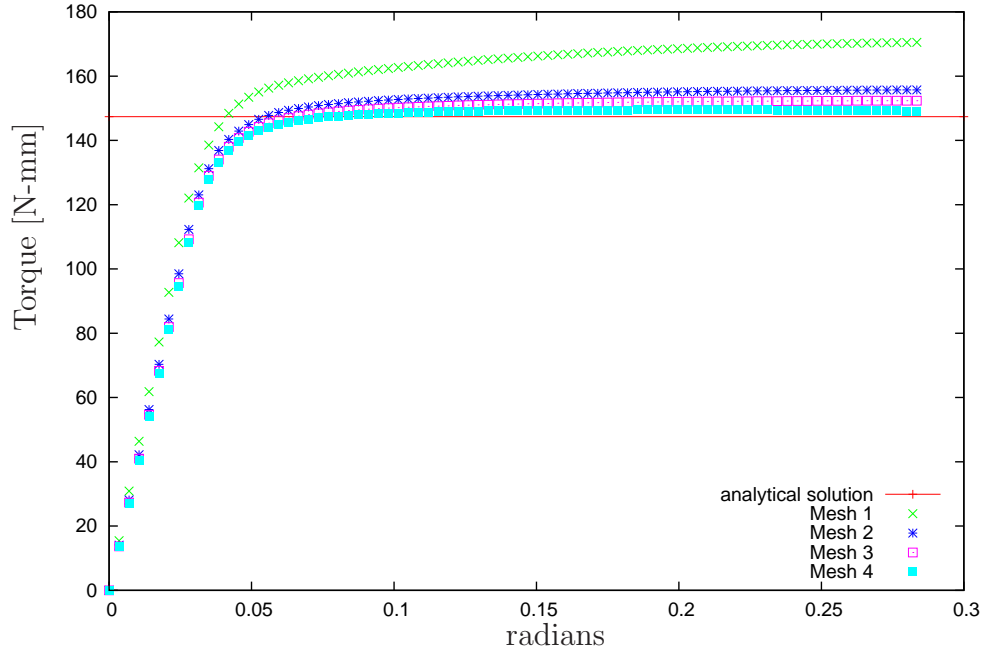


**Figure 6.2.** Perfect plasticity for the torsion BVP

The curves approach the analytical solution with mesh refinement, which shows that the computed solution is converging to the correct answer.

Next we set the hardening parameter to be non-zero. As an example, we will choose it to be  $22 * 10^3$  [MPa]. Then the same torsion BVP is solved for each of the meshes used in the perfect plasticity study, and the results can be seen in Figure 6.3. Again, note that as the mesh is refined, the curves begin to converge to one solution. It should be intuitive from Figures 6.2 and 6.3, even without the mathematical machinery of a solution convergence analysis, that classical plasticity with hardening and perfect plasticity are well-posed and well behaved.

Mesh	Number of tets
Mesh 1	1031
Mesh 2	3882
Mesh 3	12159
Mesh 4	21517

**Table 6.2.** Number of elements per mesh for the torsion BVP

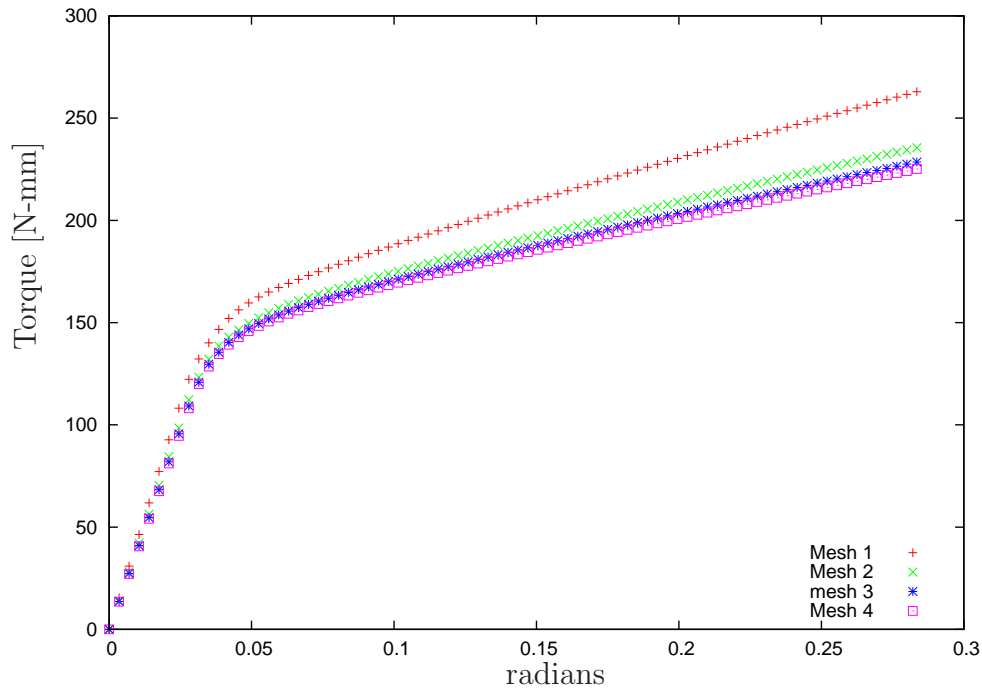


**Figure 6.3.** Isotropic hardening for the torsion BVP

When the hardening modulus becomes negative, often referred to as softening, the equations of classical plasticity are no longer well posed. This in turn leads the solution to be pathologically mesh dependent. To illustrate the idea, consider a plane strain BVP of a plate in compression. For a schematic, please refer to Figure 6.4. The plate is modeled with a geometric imperfection to force consistent localization in a band oriented at 45 deg. The same elastic properties were used as in the torsion BVP above, but now the hardening modulus is prescribed as an exponentially decreasing function of the equivalent plastic strain,  $\alpha$ . The form of the hardening modulus indicates material softening, and can be seen in (6.3).

$$K(\alpha) = 975.0 \exp(-3\alpha) \quad (6.3)$$

Figure 6.5 shows a negative slope on the load-displacement curve after the yield point, and also that as the mesh is refined, the solution no longer begins to converge to a unique solution as the slope tends to get more negative. Table 6.3 provides the number of elements used in each of the four meshes, in ascending order. This is one view of the mesh dependence associated with softening.

Another, somewhat more direct, view of the mesh dependence of softening can come from examination of the shear band produced for each mesh resolution, see Figure 6.1. The equivalent plastic strain,  $\alpha$ , was plotted on each deformed mesh, and set to the same scale for comparison. Note that there is no convergence of the shear band as the mesh is refined.

Mesh dependence in strain localization problems is a direct consequence of the fact that

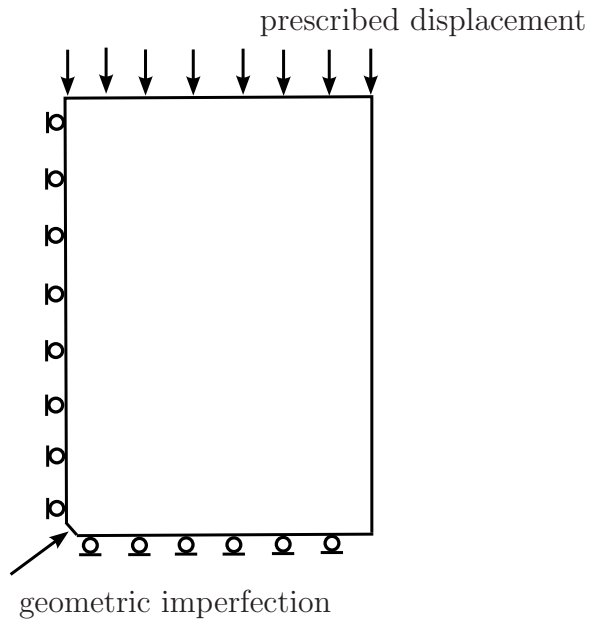


**Figure 6.4.** Schematic of the plane strain compression BVP

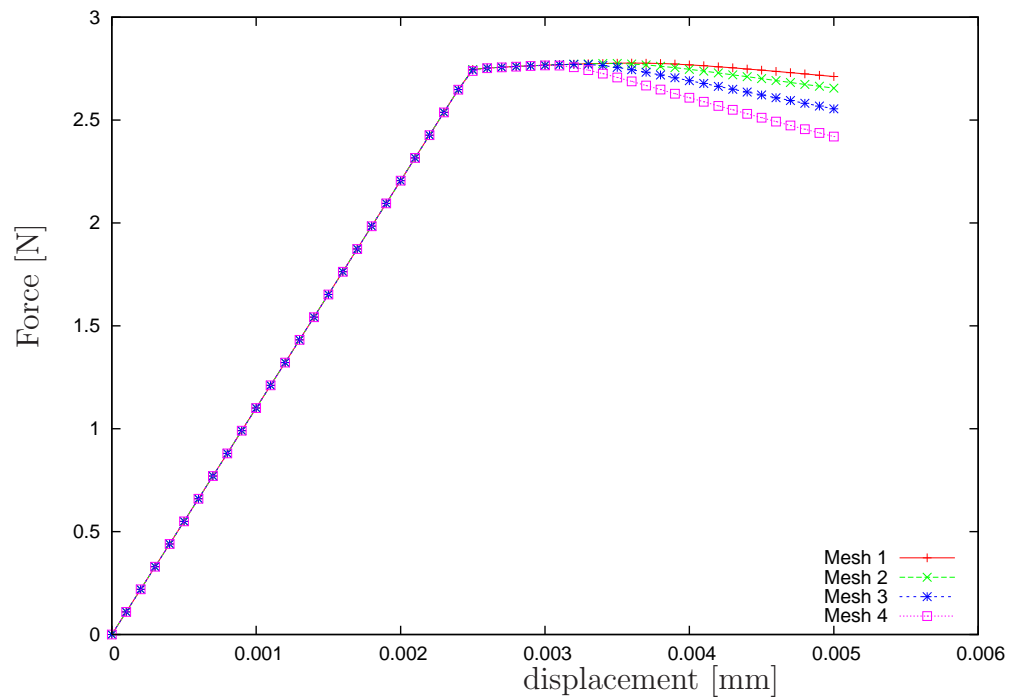


**Figure 6.5.** Softening in the plane strain compression BVP

Mesh	Number of tets
Mesh 1	3420
Mesh 2	7998
Mesh 3	37226
Mesh 4	111916

**Table 6.3.** Number of elements per mesh for the plane strain compression BVP

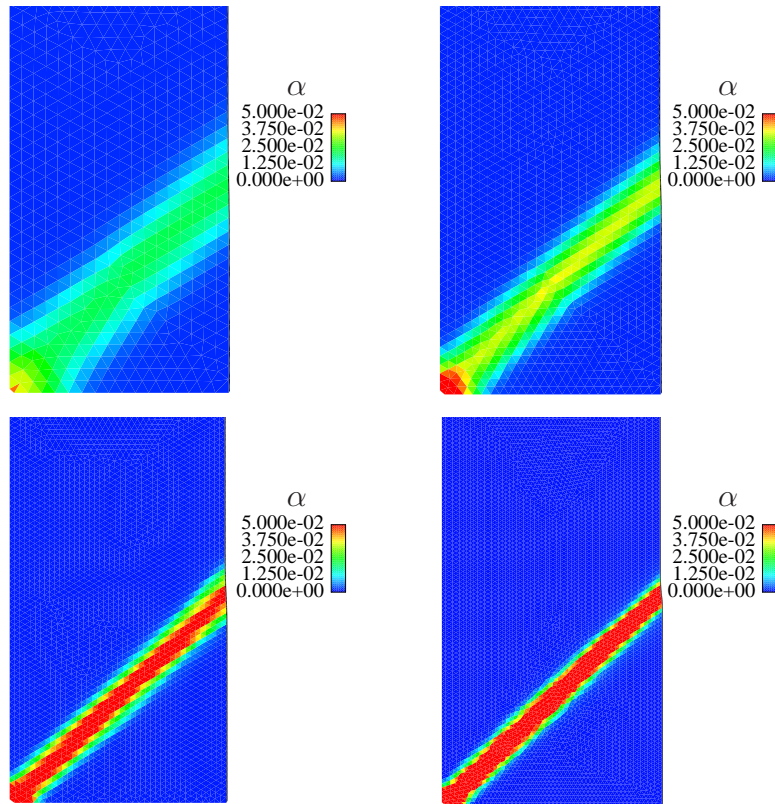


**Figure 6.6.** Equivalent plastic strain for each mesh

Mesh	Number of tets
Mesh 1	1031
Mesh 2	3882
Mesh 3	6826

**Table 6.4.** Number of elements per mesh for the DG torsion problem

the solution is not unique. The elements along the shear bands seen in Figure 6.1 introduce a length scale to the problem by which the energy associated with plastic deformation gets dissipated. Since there is no naturally occurring length scale in the continuum formulation of the problem to govern the dissipation of energy, every mesh with a different characteristic length scale will produce a different result, the very definition of mesh dependence. One interpretation of this phenomenon is an ill-posedness of strain softening problems, as the tangent modulus tensor loses *strong ellipticity*. Various methods to introduce a length scale and regularize solutions have been presented. Variational multiscale approaches are introduced in Garikipati and Hughes (1998) and Garikipati and Hughes (2000), where a fine scale is introduced to model the microstructure, and then statically condensed out. Nonlocal approaches were introduced in Bazant et al. (1984), which introduce a length scale by integrating a volume with a given radius, usually encompassing multiple element diameters. For gradient models, the introduction of another gradient, say of the plastic strain, needs some sort of length scale to remain dimensionally consistent. This length scale can then be utilized as a mechanism for energy dissipation, rendering the solution mesh independent.

## 6.2 Constant Basis for $H^p$

Implementation of the formulation using constant basis functions are now applied to the torsional BVP. Please see Figure 6.1 to recall the scenario. The first set of simulations are intended to show that as the gradient modulus,  $k$ , is varied, a proportional increase in hardening is observed. To ensure that the mesh resolution is sufficient to resolve the gradients, three meshes are used for a constant domain size and constant hardening modulus. The number of elements in each mesh used can be seen in Table 6.4, and a picture of Mesh 3 can be seen in Figure 6.7. In Figure 6.8 the relative change between the torque curves is sufficiently small to justify the use of Mesh 3 for our studies. Ideally, mesh resolutions similar to those seen above would be used in the comparison to the analytical solution for perfect plasticity would be used. However, additional computation cost introduced by the DG formulation place practical restrictions on the mesh size for the initial implementation of this model. Further refinement studies will follow more efficient implementations.

In Figure 6.9,  $k$  is varied from 0 (perfect plasticity) to 1000 [MPa-mm<sup>2</sup>] using a constant domain size and Mesh 3 from Table 6.4. The response of the model shows increased

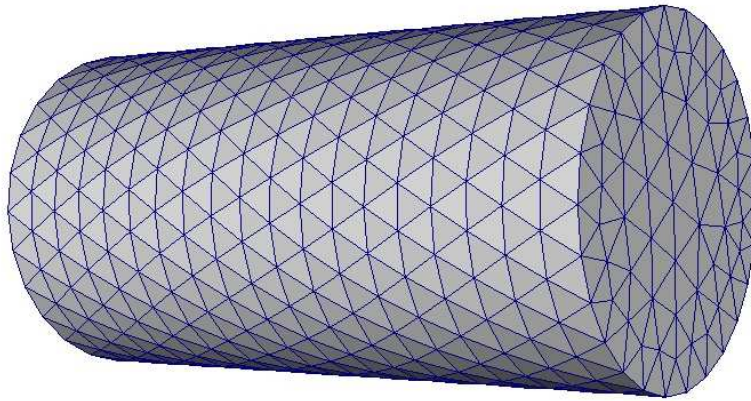


**Figure 6.7.** Picture of Mesh 3 for the DG torsion problem

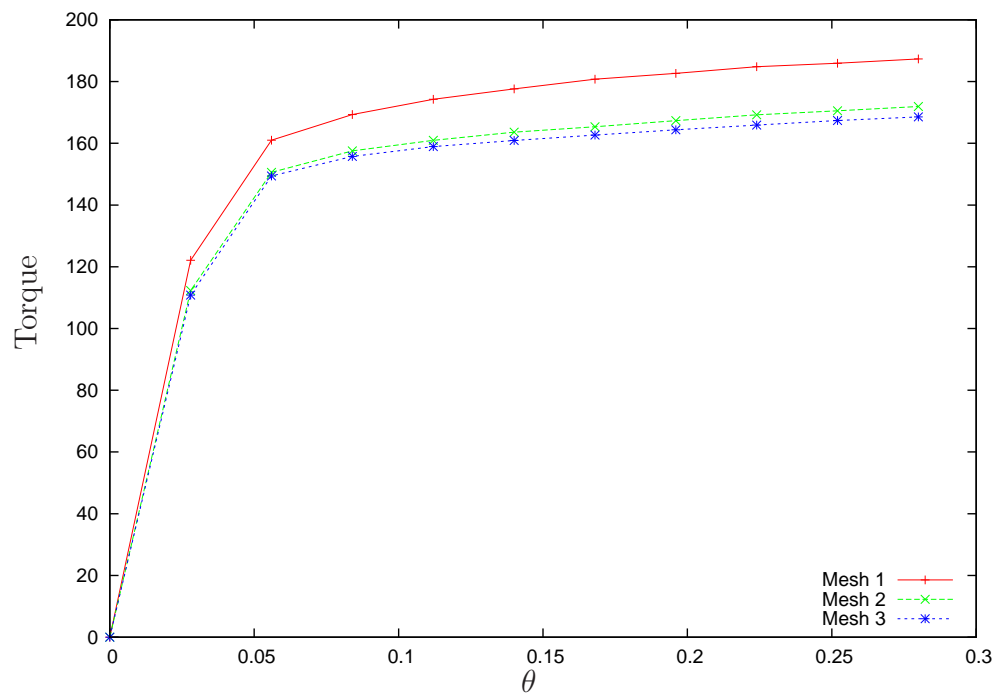


**Figure 6.8.** Hardening curve for various mesh densities

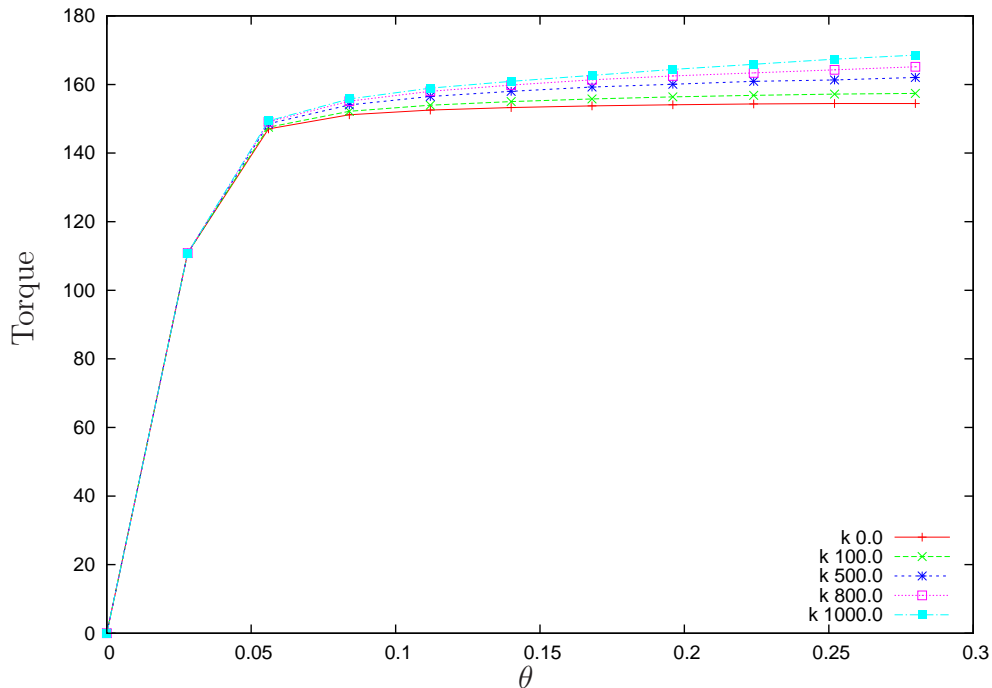


**Figure 6.9.** Influence of hardening modulus on torque versus twist

hardening, in terms of the applied torque versus twist, as  $k$  is increased.

To illustrate that the torsion problem, or another similar boundary value problem, is necessary to show the gradient dependence of the model, consider uniaxial tension. The solution will be a constant stress field throughout the domain, and the corresponding jump in  $\mathbf{H}^p$  will be zero, with a net result of zero hardening in the model. It is worth noting that for this reason, the kinematic hardening introduced in this model is not a mechanism by which to model the Bauschinger effect, discussed in Section 2.1, which can be observed in uniaxial cyclic loading. Figure 6.10 shows the lack of effect that the gradient term has on a uniaxial stress field with a gradient modulus  $k = 1000.0$ . In this case, since the hardening term is not activated, the response of the model is elastic-perfectly plastic. The number of elements for the meshes used in Figure 6.10 varied monotonically from 6 tetrahedral elements for Mesh 1 to 384 for Mesh 4 for a cubic geometry.

The first of our objectives in formulating the gradient model presented in this dissertation is the ability to model a size effect in a plastically deforming material. To accomplish this, a series of cylinders of various radius  $a$ , ranging from 1 mm to 0.125 mm, were meshed and subjected to the same torsional boundary conditions as previously discussed. Figure 6.11 shows that, for a constant gradient hardening modulus  $k=20$ , as the radius of the cylinder is decreased, the normalized hardening response increases, indicating an inverse relationship between size and hardening. The size effect cannot be captured by the classical theory, since

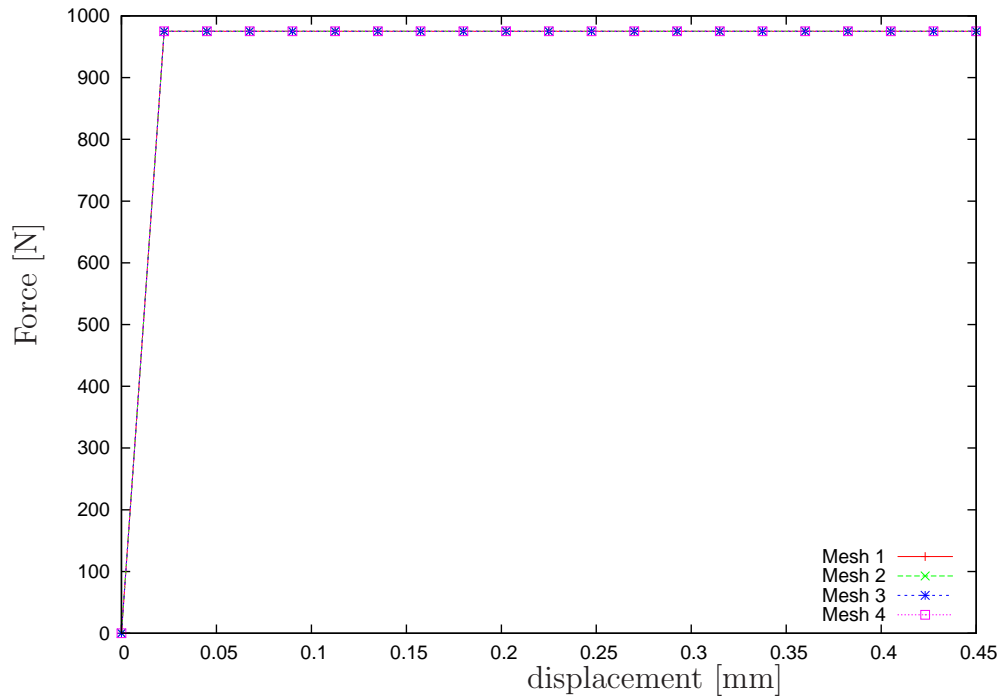


**Figure 6.10.** No hardening for model in tension

it does not include an inherent length scale.

The second main objective of the gradient formulation is the ability to achieve mesh independent solutions for localization problems. As discussed earlier, the softening pathologies can be alleviated by the introduction of a length scale by which energy can be dissipated. To this end, linear isotropic hardening is added to the gradient plasticity model. The implementation, however, differs due to the fact that the primal plastic field is now a global variable. Nevertheless, the main ideas remain the same. To show the impact that the gradient formulation has on a localization problem, we will revisit the plane strain compression problem, and apply the DG IP gradient plasticity formulation to it. See Figure 6.4 to recall the boundary value problem. The value of the linear isotropic hardening modulus used for this study is fixed at  $-2000$  MPa.<sup>1</sup> To revisit the behavior of the model with a negative linear isotropic hardening modulus, simulations were run for three different meshes, and the results can be seen in Figure 6.12, which compares with the results from the classical implementation seen in Figure 6.5. The number of elements for Meshes 1-3 correspond to the values in Table 6.3.

Introduction of a non-zero gradient modulus has the effect of introducing a length scale that serves to define a finite volume over which energy can be dissipated. For the problem under question, a gradient modulus of  $200$  [MPa-m<sup>2</sup>] is used. Figure 6.13 illustrates the

---

<sup>1</sup>As opposed to the exponential hardening law used above. The load displacement curves come out nearly the same in each case, and it should be clear that the pathology exists for both of these cases.

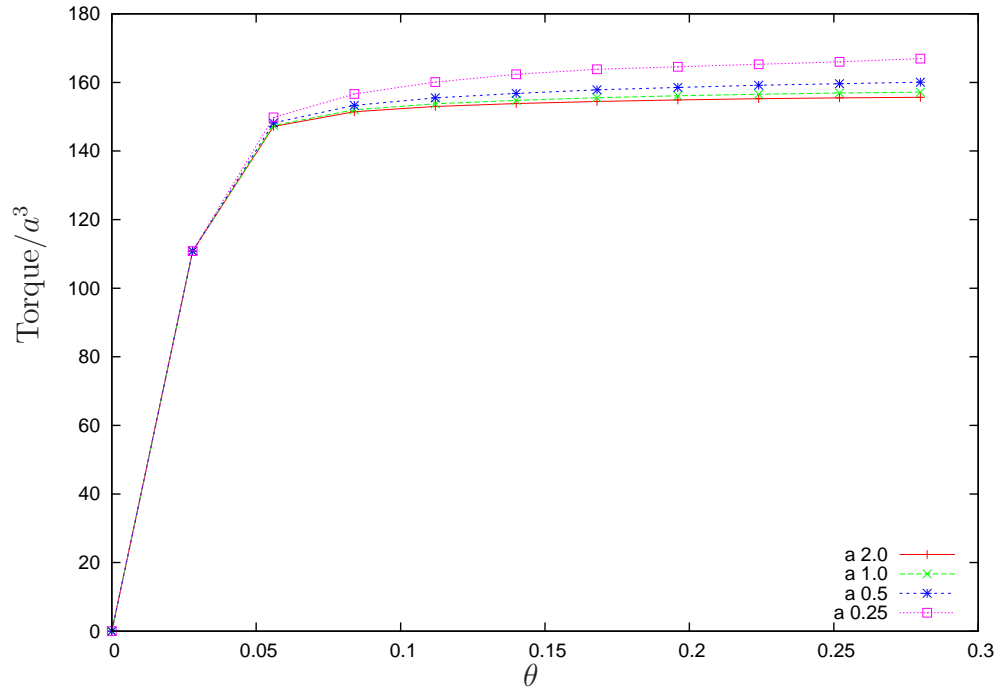


Figure 6.11. Size effect of varying the cylinder radius

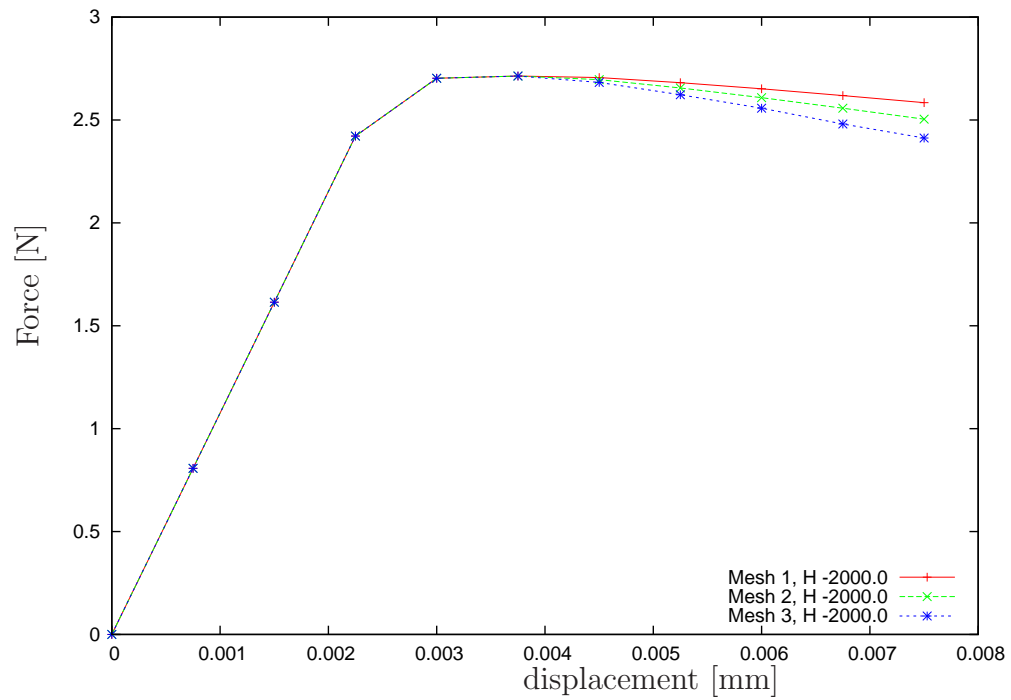
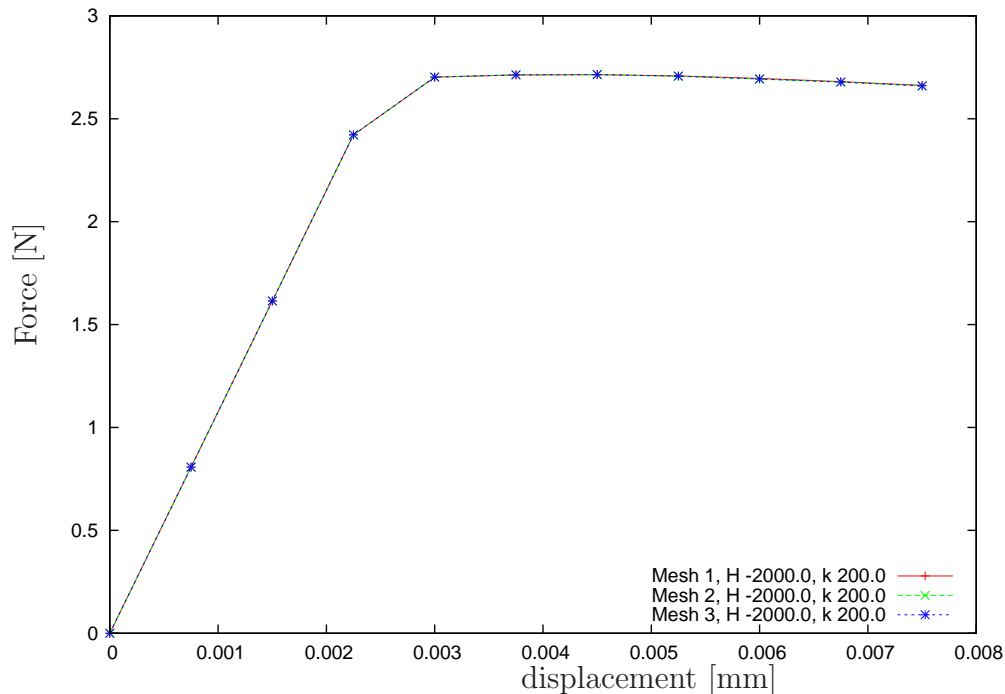


Figure 6.12. Mesh dependent softening



**Figure 6.13.** Mesh independent softening via the gradient model

effect that the gradient plasticity model has on the softening problem. The force versus displacement curves essentially lie on top of each other, providing evidence that the model does indeed alleviate the pathology associated with softening.

### 6.3 Linear Basis for $H^p$

The implementation of the linear basis for the plastic distortion is under development. Currently the mixed plasticity algorithm is being tested, and further investigation is needed. Some representative calculations are shown below for a plane strain strip of material with a circular inclusion. This particular BVP is very similar to the plane strain compression problem described above and used to illustrate softening behavior. The boundary conditions for the problem consist of fixed degrees of freedom on the bottom, constrained degrees of freedom in the horizontal direction on the face of symmetry, and prescribed displacement on the top face such that the body is globally in tension. Note that the implementation is fully three dimensional, however the problem is constrained such that there is no displacement in the out of plane direction to replicate plane strain. This BVP is interesting in that the plasticity will concentrate near the hole, and for particular choices of hardening modulus, softening will occur, yielding similarly mesh dependent solutions as shown above. Please see Figure 6.14 for the pressure field and Figure 6.15 for the equivalent plastic strain field for

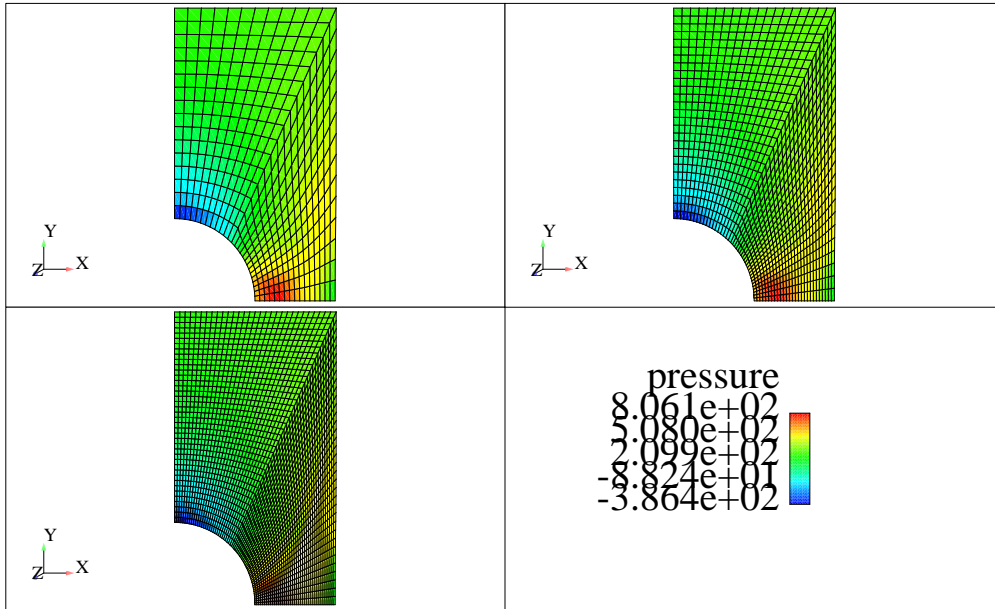


**Figure 6.14.** Pressure field in plane strain

three distinct mesh densities.

In terms of the gradient plasticity formulation using a linear basis for  $\mathbf{H}^p$ , additional difficulties arise. For the case of a constant basis, integrating the jump of a tensor field is simply the difference of the tensor field in adjacent elements. However, if a linear representation is used, the jump of a field will consist of the difference of the fields defined at the nodes comprising the element face being integrated. This necessitates, in a relative sense, considerably more attention to degree of freedom mappings and interpolations from quadrature points to nodes, and back. Since the DG implementation is being written from scratch in Matlab for the linear basis case, verification of the correctness of the computed operators takes considerably longer.

Another unresolved issue at this point deals with the application of the micro-hard and micro-free boundary conditions. Using a constant basis yields rather natural elastic-plastic boundaries at the element boundaries. In the case of a linear basis, the distinction is not so clear. In general there may be multiple integration points within an element that have exceeded the yield condition along with material points within the same element that have not yielded. It would appear that the elastic-plastic boundary would be defined within an element, making application of the boundary conditions associated with the flow rule exceedingly difficult. This stems primarily from the fact that an intra-element elastic-plastic boundary normal vector would have to be constructed. As of yet, it is unclear on the best path forward for the application of boundary conditions.

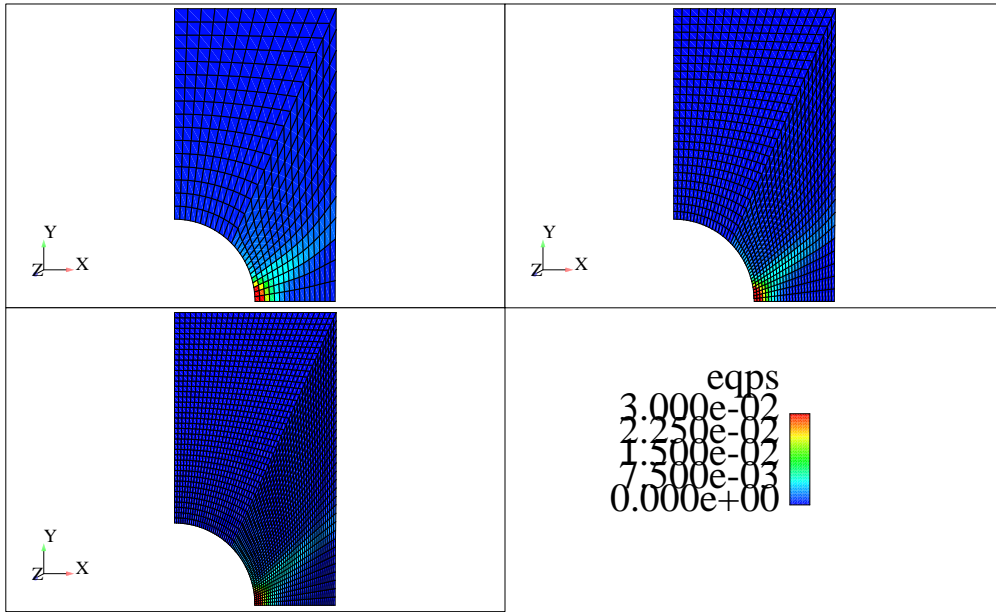


Figure 6.15. Equivalent plastic strain field in plane strain

# Chapter 7

## Conclusions

In summary, the current work presented a formulation of a gradient plasticity model cast in a discontinuous Galerkin framework. Attention was paid to the classical theory in order to illustrate the foundation of concepts central to the field of plasticity. The principles behind discontinuous Galerkin methods were discussed along with an example of the DG variational formulation in the simple setting of linear elasticity. The relationship between dislocations and plasticity, specifically dislocation motion, was examined and used as a basis for a continuum theory of a gradient dependent constitutive model. Variational principles along with the DG machinery were employed to derive a variational statement of the gradient plasticity problem fit for implementation into a nonlinear finite element code. Numerical results were generated for a select number of boundary value problems that illustrated desirable features of the proposed model, namely the ability to predict a size effect for bodies undergoing plastic deformation, and the regularization of softening problems leading to mesh independent solutions.

The tensorial nature of the flow rule proposed above differs from the standard accounts of gradient plasticity which typically only treat the scalar plastic consistency parameter, or possibly some related scalar measure. In addition, the Burgers tensor being non-symmetric adds a unknown directionality to the flow rule not present in the works in the literature. For this reason the model and method proposed here are more sophisticated than current gradient plasticity treatments. Continued effort will be spent sorting out the relevant unresolved issues outlined above.

One of the main motivations behind including a gradient term in a model of plasticity is the length scale that gets introduced. The known pathological mesh dependence of softening behavior within a numerical approximation environment can be overcome via regularization, which can take to form of adding in a material length scale parameter. The important feature of the method proposed here is the additional flow rule equation necessarily introduces a length scale into the problem, by which problems the exhibit softening can remain well posed and not exhibit mesh dependence. Another aspect of the included length scale is the ability of the model to predict the demonstrated size effect of materials at small length scales. Models of this type begin to be able to describe micro-structural phenomena, and active area of research

Once the implementation details have been sorted out in the Matlab environment, for efficiency purposes and to expand the problem size that can be attempted, the method

will have to be implemented into a parallel, high performance computing code. Ideally this implementation would be performed in the Sierra Mechanics environment, utilizing the resources Sierra provides for this type of endeavor. It is important to state that there are many unresolved issues left to be addressed at the time of this writing, and the simplicity that Matlab affords makes it a better choice to proceed with the intermediate development.

Despite the published results justifying the effort of developing a gradient plasticity theory, the search for clean, reproducible experimental methods is ongoing because of the assumptions and difficulty in handling the specimen and loading conditions at such small scales. In particular for the microtorsion experiments presented in Fleck and Hutchinson (1993), another valid explanation for the hardening response could be constructed if the grain size in the copper wires also decreased with diameter, as grain size is a known influence on the ability of a material to harden. No characterization of the grain size was discussed, so the topic is still open for debate. Experiments at these scales are not straightforward. Good results, however, are necessary for a meaningful model validation exercise. Validation entails comparisons between numerical predictions and experimental data for the purpose of determining if the correct physics have been incorporated into the model. Comparison efforts can be focused both towards legacy data found in the literature and also at results of current work.

At this time, the model presented here would not sufficiently describe the hardening response of a material in a validation exercise. To make the model generally applicable, other well known hardening mechanisms would have to be incorporated into the theory, and any future extension of the model should incorporate other mechanisms of physically motivated internal strength and back stress evolution. Also, future work entails the extension of the model into the finite deformation regime. To accomplish this, the Burgers tensor presented here will need to be extended by considering pertinent mappings between the reference, intermediate, and current configurations. Furthermore, an underlying hyperelastic model that governs the elastic response will have to be adopted.

# Bibliography

- Aifantis, E., 1987. The Physics of Plastic Deformation. *International Journal of Plasticity* 3 (3), 211–247.
- Arnold, D., Brezzi, F., Cockburn, B., Marini, L., 2002. Unified Analysis of Discontinuous Galerkin Methods for Elliptic Problems. *SIAM JOURNAL ON NUMERICAL ANALYSIS* 39 (5), 1749–1779.
- Asaro, R., 1983. Crystal plasticity. *Journal of applied mechanics* 50 (4 B), 921–934.
- Bassi, F., Rebay, S., 1997. A High-Order Accurate Discontinuous Finite Element Method for the Numerical Solution of the Compressible Navier-Stokes Equations. *J. Comput. Phys.* 131 (2), 267–279.
- Bazant, Z., Pijaudier-Cabot, G., 1988. Nonlocal continuum damage, localization instability and convergence. *Journal of Applied Mechanics* 55 (2), 287–293.
- Bazant, Z. P., Belytschko, T. B., Chang, T. P., 1984. Continuum Theory for Strain Softening. *Journal of Engineering Mechanics* 110, 1666–1691.
- Brezzi, F., 1990. A discourse on the stability conditions for mixed finite element formulations. *Comp. Methods in Applied Mech. Engrg.* 82 (1-3), 27–57.
- Cermelli, P., Gurtin, M., 2001. On the characterization of geometrically necessary dislocations in finite plasticity. *Journal of Mechanics and Physics of Solids* 49 (7), 1539–1568.
- Coleman, B., Hodgdon, M., 1985. On shear bands in ductile materials. *Archive for Rational Mechanics and Analysis* 90 (3), 219–247.
- Djoko, J., Ebobisse, F., McBride, A., Reddy, B., 2007a. A discontinuous galerkin formulation for classical and gradient plasticity - part 1: Formulation and analysis. *Comp. Methods in Applied Mech. Engrg.* 196, 3881–3897.
- Djoko, J., Ebobisse, F., McBride, A., Reddy, B., 2007b. A discontinuous galerkin formulation for classical and gradient plasticity - part 2: Algorithms and numerical analysis. *Comp. Methods in Applied Mech. Engrg.* 197, 1–21.
- Engel, G., Garikipati, K., Hughes, T. J. R., Larson, M. G., Mazzei, L., Taylor, R. L., 2002. Continuous/Discontinuous Finite Element Approximations of Fourth-order Elliptic Problems in Structural and Continuum Mechanics with Applications to Thin Beams and Plates, and Strain Gradient Elasticity. *Comp. Methods in Applied Mech. Engrg.* 191 (34), 3669–3750.

- Fleck, N. A., Hutchinson, J. W., 1993. A Phenomenological Theory for Strain Gradient Effects in Plasticity. *Journal of Mechanics and Physics of Solids* 12, 1825–1857.
- Fleck, N. A., Muller, G. M., Ashby, M. F., Hutchinson, J. W., 1994. Strain Gradient Plasticity: Theory and Experiment. *Acta Metallurgica et Materialia* 42, 475–487.
- Gao, H., Huang, Y., Nix, W. D., 1999. Mechanism-based Strain Gradient Plasticity–I. Theory. *Journal of Mechanics and Physics of Solids* 47, 789–828.
- Garikipati, K., Hughes, T., 1998. A study of strain localization in a multiple scale framework - the one-dimensional problem. *Comp. Methods in Applied Mech. Engrg.* 159 (3-4), 193–222.
- Garikipati, K., Hughes, T., 2000. A variational multiscale approach to strain localization-formulation for multidimensional problems. *Comp. Methods in Applied Mech. Engrg.* 188 (1–3), 39–60.
- Gurtin, M., 2004. A gradient theory of small-deformation isotropic plasticity that accounts for the burgers vector and for dissipation due to plastic spin. *Journal of Mechanics and Physics of Solids* 52, 2545–2568.
- Gurtin, M., 2005. A theory of strain-gradient plasticity for isotropic, plastically irrotational materials. part i: Small deformations. *Journal of Mechanics and Physics of Solids* 53, 1624–1649.
- Hill, R., 1950. *The Mathematical Theory of Plasticity*. Oxford University Press.
- Huang, Y., Gao, H., Nix, W., Hutchinson, J., 2000. Mechanism-based strain gradient plasticity-II. Analysis. *Journal of Mechanics and Physics of Solids* 48 (1), 99–128.
- Hughes, T. J. R., 1987. *The Finite Element Method*. Prentice-Hall, Englewood-Cliffs, N. J.
- Kachanov, L. M., 1971. *Foundations of the Theory of Plasticity*. North Holland Publishing Co.
- Key, S. W., Krieg, R. D., 1982. On the numerical implementation of inelastic time dependent and time independent, finite strain constitutive equations in structural mechanics. *Comp. Methods in Applied Mech. Engrg.* 33 (1-3), 439 – 452.
- Krieg, R., Key, S., 1976. Implementation of a time independent plasticity theory into structural computer programs. *Constitutive equations in viscoplasticity: Computational and engineering aspects* , 125–137.
- Kroner, E., Teodosiu, C., 1972. Lattice defect approach to plasticity and viscoplasticity. In: Sawczuk, A. (Ed.), *Problems of Plasticity*. Noordhoff.
- Lee, E. H., 1969. Elastic-Plastic Deformation at Finite Strains. *J. Applied Mechanics* 36, 1–6.
- Lubliner, J., 1990. *Plasticity Theory*. Macmillan Publishing Co.

- Ma, Q., Clarke, D., 1995. Size dependent hardness of silver single crystals. *Journal of Materials Research* 10 (4), 853–863.
- McBride, A. T., 2008. Formulation, analysis and solution algorithms for a model of gradient plasticity within a discontinuous Galerkin framework. Ph.D. thesis, University of Cape Town.
- Molari, L., Wells, G. N., Garikipati, K., Ubertini, F., 2006. A discontinuous Galerkin method for strain gradient-dependent damage: Study of interpolations, convergence and two dimensional problems. *Comp. Methods in Applied Mech. Engrg.* 195, 1480–1498.
- Muhlhaus, H., Aifantis, E., 1991. A variational principle for gradient plasticity. *Int. J. Solids and Structures* 28 (7), 845–857.
- Nitsche, J., 1971. Über ein Variationsprinzip zur Lösung von Dirichlet-Problemen bei Verwendung von Teilräumen, die keinen Randbedingungen unterworfen sind [On a variational principle for solving Dirichlet problems less boundary conditions using subspaces]. *Abh. Math. Sem. Univ. Hamburg* 36, 9–15.
- Nix, W. D., Gao, H., 1998. Indentation Size Effects in Crystalline Materials: A Law for Strain Gradient Plasticity. *Journal of Mechanics and Physics of Solids* 46, 411–425.
- Noels, L., Radovitzky, R., 2008. An explicit discontinuous galerkin method for non-linear solid dynamics: Formulation, parallel implementation and scalability properties. *Int. J. Numer. Methods Engrg.* 74, 1393–1420.
- Ortiz, M., Simo, J., 1986. An analysis of a new class of integration algorithms for elastoplastic constitutive relations. *Int. J. Numer. Methods Engrg.* 23 (3).
- Reed, W., Hill, T., 1973. Triangular mesh methods for the neutron transport equation. In: *National topical meeting on mathematical models and computational techniques for analysis of nuclear systems*. Vol. 8.
- Simo, J. C., 1988a. A Framework for Finite Strain Elastoplasticity based on Maximum Plastic Dissipation and the Multiplicative Decomposition: Part I. Continuum Formulation. *Comp. Methods in Applied Mech. Engrg.* 66, 199–219.
- Simo, J. C., 1988b. A Framework for Finite Strain Elastoplasticity based on Maximum Plastic Dissipation and the Multiplicative Decomposition: Part II. Computational Aspects. *Comp. Methods in Applied Mech. Engrg.* 68, 1–31.
- Simo, J. C., 1992. Algorithms for Multiplicative Plasticity that Preserve the form of the Return Mappings of the Infinitesimal Theory. *Comp. Methods in Applied Mech. Engrg.* 99, 41–104.
- Simo, J. C., 1998. Numerical Analysis of Simulation of Plasticity. In: Ciarlet, P. G., Lions, J. L. (Eds.), *Handbook of Numerical Analysis*, Vol. VI. Elsevier, pp. 183–499.
- Simo, J. C., Hughes, T. J. R., 1998. *Computational Inelasticity*. Springer Verlag.

- Stölken, J., Evans, A., 1998. A microbend test method for measuring the plasticity length scale. *Acta Materialia* 46 (14), 5109–5115.
- Taylor, G. I., 1938. Analysis of Plastic Strain in a Cubic Crystal. In: Lessels, J. M. (Ed.), Stephen Timoshenko. 60th Anniversary Volume. Macmillan, New York.
- Wells, G., Dung, N., 2007. A  $c^0$  discontinuous galerkin formulation for kirchhoff plates. *Comp. Methods in Applied Mech. Engrg.* 196, 3370–3380.
- Wells, G., Kuhl, E., Garikipati, K., 2006. A discontinuous galerkin method for the cahn-hilliard equation. *J. Comput. Phys.* 218, 860–877.
- Wells, G. N., Garikipati, K., Molari, L., 2004. A discontinuous Galerkin formulation for a strain gradient-dependent damage model. *Comp. Methods in Applied Mech. Engrg.* 193, 3633–3645.
- Wilkins, M., 1963. Calculation of elastic-plastic flow. UCRL-7322 (Rev. 1), California Univ., Livermore. Lawrence Radiation Lab.
- Zienkiewicz, O. C., Taylor, R. L., 1989. *The Finite Element Method: Vol I and II*. McGraw-Hill, London, New York.

## DISTRIBUTION:

- 1 Prof. Krishna Garikipati  
Department of Mechanical Engineering  
University of Michigan  
2350 Hayward Street  
Ann Arbor, MI 48109
  
- 1 MS 0372 Jake Ostien, 8246
- 1 MS 0372 Bill Scherzinger, 1524
- 1 MS 0372 Kevin Long, 1524
- 1 MS 0372 Eliot Fang, 1524
- 1 MS 0372 Jay Foulk, 8246
- 1 MS 0372 Alejandro Mota, 8246
- 1 MS 0372 Jonathon Zimmerman, 8246
- 1 MS 0372 Mike Chiesa, 8249
- 1 MS 0899 Technical Library, 9536 (electronic copy)





